FINITE ELEMENT BASED VIBRATION AND STABILITY ANALYSIS OF FUNCTIONALLY GRADED ROTATING SHAFT SYSTEM UNDER THERMAL ENVIRONMENT

A THESIS SUBMITTED IN THE PARTIAL FULFILLMENT OF THE REQUIREMENTS FOR THE DEGREE OF

Master of Technology

In

MECHANICAL ENGINEERING

[Specialization: Machine Design and Analysis]

By

Debabrata Gayen

211ME1156

Department Of Mechanical Engineering

National Institute of Technology Rourkela

Rourkela, Orissa, India – 769008

June, 2013

FINITE ELEMENT BASED VIBRATION AND STABILITY ANALYSIS OF FUNCTIONALLY GRADED ROTATING SHAFT SYSTEM UNDER THERMAL ENVIRONMENT

A THESIS SUBMITTED IN THE PARTIAL FULFILLMENT OF THE REQUIREMENTS FOR THE DEGREE OF

Master of Technology

In

MECHANICAL ENGINEERING

[Specialization: Machine Design and Analysis]

By

Debabrata Gayen

211ME1156

Under the Supervisions of

Prof. T. Roy and Prof. A. Mitra

Department Of Mechanical Engineering

National Institute of Technology Rourkela

Rourkela, Orissa, India – 769008

June, 2013

NATIONAL INSTITUTE OF TECHNOLOGY ROURKELA

CERTIFICATE

*This is to certify that the thesis entitled, "**Finite Element Based Vibration and Stability Analysis of Functionally Graded Rotating Shaft System Under Thermal Environment**", being submitted by **Mr. DEBABRATA GAYEN** in partial fulfillment of the requirements for the award of **"MASTER OF TECHNOLOGY"** Degree in **"MECHANICAL ENGINEERING"** with specialization in **"MACHINE DESIGN AND ANALYSIS"** at the National Institute of Technology Rourkela (India) is an authentic Work carried out by him under our supervisions.*

To the best of our knowledge, the results embodied in the thesis has not been submitted to any other University or Institute for the award of any Degree or Diploma.

Supervisor

(Prof. T. Roy)
Department of Mechanical Engineering
National Institute of Technology Rourkela
Orissa, India- 769008.

Co - Supervisor

(Prof. A. Mitra)
Department of Mechanical Engineering
National Institute of Technology Rourkela
Orissa, India- 769008.

ACKNOWLEDGEMENTS

First and foremost, I wish to express my sense of gratitude and indebtedness to my supervisors, Prof. Tarapada Roy and Prof. Anirban Mitra for their inspiring guidance, encouragement, and untiring efforts throughout the course of this work. Their timely help, constructive criticism and painstaking efforts made it possible to present the work contained in this thesis.

Specially, I extend my deep sense of indebtedness and gratitude to Prof. Tarapada Roy for his kindness in providing me an opportunity to work under his supervision and guidance. He played a crucial role in the process of my research work. First of all, he allowed me to join his research group; even two scholars were working under him. His advice to harmonize theory and applications help me a lot in my research. He showed me different ways to approach a research problem and the need to be persistent to accomplish my goal. His keen interest, invaluable guidance and immense help have helped me for the successful completion of the thesis.

After the completion of this Thesis, I experience a feeling of achievement and satisfaction. Looking into the past I realize how impossible it was for me to succeed on my own. I wish to express my deep gratitude to all those who extended their helping hands towards me in various ways during my tenure at NIT Rourkela. I greatly appreciate and convey my heartfelt thanks to my colleagues 'flow of ideas, dear ones and all those who helped me in the completion of this work. The beautiful weather of NIT Campus, kept me in good health and high spirits throughout the research period.

I am also thankful to Prof. K. P. Maity, Head of the Department, Mechanical Engineering, for his moral support and valuable suggestions regarding the research work.

I am especially indebted to my parents for their love, sacrifice and support. They are my first teachers after I came to this world and have set great examples for me about how to live, study and work.

DEBABRATA GAYEN

Roll No. 211MEE1156

Department of Mechanical Engineering

National Institute of Technology Rourkela

Orissa, India- 769008.

Table of Contents

List of Tables

List of Figures

Abstract

The present work deals with the study of vibration and stability analyses of functionally graded (FG) spinning shaft system under thermal environment using three nodded beam element based on Timoshenko beam theory (TBT). Temperature field is assumed to be a uniform distribution over the shaft surface and varied in radial direction only. Material properties are assumed to be temperature dependent and graded in radial direction according to power law gradation and exponential law gradation respectively. In the present analysis, the mixture of Aluminum Oxide (Al_2O_3) and Stainless Steel (SUS304) is considered as FG material where metal contain (SUS304) is decreasing towards the outer diameter of shaft. The FG shafts are modeled as a Timoshenko beam by mounting discrete isotropic rigid disks on it and supported by flexible bearings that are modeled with viscous dampers and springs. Based on first order shear deformation (FOSD) beam theory with transverse shear deformation, rotary inertia, gyroscopic effect, strain and kinetic energy of shafts are derived by adopting three-dimensional constitutive relations of material. The derivation of governing equation of motion is obtained using Hamilton's principle and solutions are obtained by three-node finite element (FE) with four degrees of freedom (DOF) per node. . In this work the effects of both internal viscous and hysteretic damping have also been incorporated in the finite element model. A complete code has been developed using MATLAB program and validated with the existing results available in literatures. The analysis of numerical results reveals that temperature field and power law gradient index have a significance role on the materials properties (such as Young modulus, Poisson ratio, modulus of rigidity, coefficient of thermal expansion etc.) of FG shaft. Various results have also been obtained such as Campbell diagram, stability speed limit (SLS), damping ratio and time responses for FG shaft due unbalance masses and also compared with conventional steel shaft. It has been found that the responses of the FG spinning shaft are significantly influenced by radial thickness, power law gradient index and internal (viscous and hysteretic) damping and temperature dependent material properties. The obtained results also show that the advantages of FG shaft over conventional steel shaft.

Keywords: Power law gradient index; Functionally graded shaft; Temperature dependent material properties; Viscous and hysteretic damping; Rotor-Bearing-shaft system; Finite element method; Campbell diagram; Damping ratio; stability speed limit (SLS)

CHAPTER 1

INTRODUCTION

Composite materials and structures are more and more frequently used in advanced engineering fields mainly because of their high stiffness-to-weight ratio that is particularly favorable. However the main downside of composite materials is represented by the weakness of interfaces between adjacent layers known as delimitation phenomena that may lead to structural failure. To partially overcome these problems, a new class of materials named Functionally Graded Materials (FGMs) has recently been proposed whose various material properties vary through the radial and thickness direction in a continuous manner and thus free from interface weakness. The gradation of material properties reduces thermal stresses, residual stresses, and stress concentrations. A functionally graded structure is defined as, those in which the volume fractions of two or more materials are varied continuously as a function of position along certain dimension (typically the radius and thickness) of the structure to achieve a require function. FGMs can provide designers with tailored material response and exceptional performance in thermal environments. For example, the Space Shuttle utilizes ceramic tiles as thermal protection from heat generated during re-entry into the Earth's atmosphere. An FGM composed of ceramic on the outside surface and metal on the inside surface.

Due to high strength, high stiffness, and low density characteristics, FGMs rotor shafts have been sought as new potential candidates for replacement of the conventional metallic shafts in many application areas for the design of rotating mechanical components such as, driveshaft for helicopters and cars and jet engine, commercial and military rotating machines, aerospace and space vehicles etc. In Rotor-dynamic applications, composites have been demonstrated both numerically and experimentally. Accompanied by the development of many new advance composite materials and various mathematical models of rotor-shafts were also developed by researchers.

1.1 Background and Importance of Rotor Dynamic

Rotor dynamics has a remarkable history, largely due to the interplay between its theory and its practice. **Rotor dynamics** is a specialized branch of applied mechanics concerned with the behavior and diagnosis of rotating structures. It is commonly used to analyze the behavior of structures ranging from jet engines and steam turbines to auto engines and computer disk storage. Basic level of Rotor Dynamic is concerned with rotor and stator. Rotor is a rotating part of a mechanical device or structures supported by bearings and influenced by internal phenomena that rotate freely about an axis fixed in space. Engineering components concerned with the subject of rotor dynamics are rotors in machines, especially of turbines, generators, motors, compressors, blowers, alternators, pumps, brakes, distributors and the like.

Rotor provides with materials bearings to constrain their spin axis in a more or rigid way to a fixed position in space, are referred to as fixed rotor (which consider spin speed is constant), where as those that are not considered in any way are referred free rotor (which consider spin speed is governed by conservation of angular momentum). In operation Rotors have a great deal of rotational energy and a small amount of vibrational (bending, axial and torsional) energy.

In Rotor Dynamics field William John Macquorn Rankine (1869) performed the first analysis of a spinning shaft. He chose a two-degrees-of-freedom model consisted of a rigid mass whirling in an orbit, with elastic spring acting in the radial direction. He defined the whirling speed of the shaft but he can be shown that beyond this whirling speed the radial deflection of Rankine's model increases without limit and this speed is called threshold speed for the divergent instability.

In 1883 Swedish engineer Carl Gustaf Patrik de Laval developed a single-stage steam impulse turbine for marine applications and succeeded in its operation at 42,000 rpm. He first used a rigid rotor, but latter used a flexible rotor and shown that it was possible to operate above critical speed by operating at a rotational speed about seven times the critical speed.

In 1895, Stanley Dunkerley published a study of the vibration of shafts loaded by pulleys. The first sentence of his paper reads, "It is well known that every shaft, however nearly balanced, when driven at a particular speed, bends, and, unless the amount of deflection is limited, might even break, although at higher speeds the shaft again runs true. This particular speed or 'critical speed' depends on the manner in which the shaft is supported, its size and modulus of elasticity, and the sizes, weights, and positions of any pulleys it carries." In 1895 German civil engineer August Foppl who showed that an alternate rotor model exhibited a stable solution above Rankine's whirling speed. In England W. Kerr (1916) published experimental evidence that a second "critical speed" existed and it was obvious to all that a second critical speed could only be attained by the safe traversal of the first critical speed. In 1918 Ludwig Prandtl was the first to study a Jeffcott rotor with a non-circular cross-section.

In 1919, Henry Jeffcott modeled a simple rotor to study the flexural behavior of rotors and dynamic behavior in “The lateral vibration of loaded shafts in the neighborhood of a whirling speed-the effect of want of balance,” It is often referred to as Jeffcott rotor. But Jeffcott's analytical model the disk did not wobble. As a result, the angular velocity vector and the angular momentum vector were collinear and no gyroscopic moments were generated.

However, this attribution is incorrect and Föppl (1895) published “Das problem der laval’shen turbinewelle,” in which its behavior is correctly analyzed. After that Jeffcott confirmed Foppl's prediction that a stable supercritical solution existed and he extended Foppl's analysis by including external damping.

In 1924 Aurel B. Stodola removed the Jeffcott's restriction and developed dynamics of elastic shaft with discs and continuous rotors without considering gyroscopic moment, the secondary resonance phenomenon due to gravity effect, the balancing of rotors, and methods of determining approximate values of critical speeds of rotors with variable cross sections, supercritical solutions were stabilized by Coriolis accelerations.

Then Baker (1933) described self-excited vibrations due to contact between rotor and stator. In 1933 David M. Smith obtained simple formulas that predicted how the threshold spin speed for supercritical instability varied with bearing stiffness and with the ratio of external to internal viscous damping.

Gradually, the Jeffcott rotor model with many variations came closer to the practical needs of the rotor dynamic field of the day. But, not close enough. In 1945 Prohl's and Myklestad's work led the Transfer Matrix Method (TMM) for analyzing instabilities and modeling techniques of rotors.

After World War II, rotor dynamics had become an international endeavor, and recognized by the Rotor Dynamics Committee of the International Federation of the Theory of Machines and Mechanisms (IFToMM) and beginning in Rome (1982), Tokyo (1986), Lyon (1990), Chicago (1994), Darmstadt (1998), Sydney (2002), and Vienna (2006).

For revolution in solution capability, In the 1960s numerical methods developed for structural dynamics analysis and digital computer codes and rotor dynamics codes was based on the TMM method but in the 1970s another underlying algorithm, the Finite Element Method (FEM), became available for the solution of the prevailing beam-based models. Now, in the beginning of the 21st century, rotor dynamics are combining the FEM and solids modeling techniques to generate simulations that accommodate the coupled behavior of flexible disks, flexible shafts and flexible support structures into a single, massive, multidimensional-model.

1.2 Composite Materials

Composite materials are formed by combining two or more material on a micro scale form and their constituents do not dissolve or merge into each other, to achieve superior enhanced properties. These are widely used in a variety of structures, including army and aerospace vehicles, nuclear reactor vessels, turbines parts, buildings and smart highways (i.e. civil infrastructure applications) as well in sports equipment and medical prosthetics. Laminated composite structures consist of several layers of different fiber-reinforced laminate bonded together to obtain desired structural properties (e.g. stiffness, strength, wear resistance, CTE, Thermal conductivity, damping, and so on). Varying the lamina thickness, lamina material properties, and stacking sequence desired structural properties can be achieved. The increased use of laminated composites in various types of structures led to considerable interests in their analysis. Composite materials exhibit high strength-to weight and stiffness-to-weight ratios, which make them ideally suited for use in weight sensitive

structures. This weight reduction of structures leads to improvement of their structural performance, especially in space applications.

1.3 Drawback of Composite Materials

Though laminated composites give numerous advantages over conventional materials, their major downside is however represented by the repeated cyclic stress, impact load and so on can causes to separate layers and weakness of interfaces between adjacent layers, known as delamination phenomena (i.e. Mode of failure or failure mechanisms of composite materials). It may lead to failure of the structure. Additional problems include the presence of residual stresses due to the difference in coefficient of thermal expansion and coefficient of moisture expansion of the fiber and matrix. For anisotropic constitution of laminated composite structures often results in stress concentrations near material and geometric interface that can lead to damage in the form of de-lamination, matrix cracking and adhesive bond separation. These problems can be reduced if the sudden change of material properties is somehow prevented.

1.4 Conceptual Idea about FGMs

First FGM concepts have come from Japan in 1984 during a space plane project. There a combination of materials used would serve the purpose of a thermal barrier capable of withstanding a surface temperature of 2000 K and a temperature gradient of 1000 k across a 10 mm section. Recently FGMs concept has become more popular in Europe (Germany). A collaborative research center Transregio (SFB Transregio) is funded since 2006 in order to exploit the potential of grading mono-materials, such as steel, aluminum and polypropylene, by using thermo mechanically coupled manufacturing processes

Functionally Graded Materials (FGMs) are those composite materials where the composition or the microstructure is locally varied so that a certain variation of the local material properties is achieved. FGM is also defined as, those in which the volume fraction of two or more materials are achieved continuously as a function of position along certain directions of the structure to achieve a required function (e.g. mixture of ceramic and metal). It is materially heterogeneous which is defined for those objects with and/or multiple material objects with clear material domain. By grading of material properties in a continuous manner, the effect of inter-laminar stresses developed at the interfaces of the laminated composite due to abrupt change of material properties between neighboring laminas is mitigated.

As many thin walled members, i.e., plates and shells used in reactor vessels, turbines and other machine parts are susceptible to failure from buckling, large amplitude deflections, or excessive stresses induced by thermal or combined thermo mechanical loading. Thus, FGMs are primarily used in structures subjected to extreme temperature environment or where high temperature gradients are encountered. Mainly they are manufactured from isotropic components such as metals and ceramics, since role of metal portion is acts as structure support while ceramics provides thermal protection in environments with severe

thermal gradients (e.g. reactor vessels, semiconductor industry).In such conditions ceramic provides heat and corrosion resistance, while the metal provides the strength and toughness.

Whatever problems arises in using composite materials those problems can be reduced significantly by using FGMs instead of composite materials because FGMs changes the material properties from surface to surface or layer to layer. FGMs are new advanced multifunctional composites where volume fractions of the reinforcements phase(s) vary smoothly. Additionally, FGM allows the certain superior and multiple properties without any mechanically weak interface. This new concept of materials hinges on materials science and mechanics due to integration of the material and structural considerations into the final design of structural component. Moreover, gradual change of properties can be tailored to different applications and service environments.

1.5 Applications of FGMs

Due to progressing of technology it is need for advanced capability of materials to become a priority in engineering field for higher performance systems. FGMs are relatively new materials and are being studied for the use in high temperature applications. FGM is an extensive variety of applications in engineering practice which requires materials performance to vary with locations within the component. The following applications are noticeable such as,

1) Aerospace field (space planes, space structures, nuclear reactors, insulations for cooling structures, Aerospace skins, Rocket engine components, Vibration control, Adaptive structures etc.).
2) Engineering field (Turbine blade, shaft, cutting tool etc.)
3) Optical field (optical fiber, lens etc.)
4) Electronics field (sensor, graded band semiconductor, substrate etc.)
5) Chemical field (Heat Exchanger, Reactor Vessel, Heat Pipe etc.)
6) Biomaterial field (artificial skin, drug delivery system, prosthetics etc.)
7) Commodities (Building materials, Sports good, Car body etc.)
8) Energy conversion (Thermoelectric generator, Thermo ionic converter, Fuel cells, Solar cells etc.)
9) Optoelectronics
10) Piezoelectricity

1.6 Outline of the Present Work

The outline of this thesis is divided into six chapters. Chapter 1 presents an introduction of composite material, FG materials and also brief introduction to rotor dynamics. The outline of the present work is also given in the Chapter 1.

Then Chapter 2 provides a state of the art of composite materials structure, functionally graded materials structure and vibration and control of spinning shaft systems.

In Chapter 3 represents the modeling of FG material to obtain the effective material properties of FG shaft.

Chapter 4 presents a detailed formulation of the governing equations of spinning rotor shaft system for analyzing vibration and stability of FGMs. Formulations of the equations of motion are developed for a first order shear deformable beam by contributing internal damping.

Chapter 5 discusses the results of the analyses performed in this project work and detailed report of results and discussion has been given. Various type of analysis for FG shaft have been studied and presented. Finally, Chapter 6 summarizes conclusions of this project work and scopes for further work are suggested.

CHAPTER 2

REVIEW OF RELEVANT LITERATURES

2.1 Introduction

Numerous research works have been done in the field of modeling and analysis of functionally graded (FG) structures. Some important works based on the different analysis have been presented in the following sections. Advanced composite materials offer numerous superior properties over metallic materials, like high specific strength and high specific stiffness. This has resulted in the extensive use of laminated composite materials in aircraft, spacecraft and space structures. In an effort to develop the super heat resistant materials, Koizumi [1] first proposed the concept of FGM. These materials are microscopically heterogeneous and are typically made from isotropic components, such as metals and ceramics. After the concept of FGMs was set by the Japanese school of material science and confirmation of their potentials several branches of research originated and are still being broadened by research groups all over the world.

2.2 Composite Materials Structure

Zinberg and Symonds [2] investigated the model of rotating anisotropic shafts and compared the critical speeds of composite shaft over aluminum alloy shaft by using equivalent modulus beam theory (EMBT). Nelson et al. [3] and Nelson [4] contributed a substantial improvement in the computational analysis of rotating shafts incorporating the effect of gyroscopic, rotary inertia, moment and shear deformation into the FE shafts model. Rouch et al. [5] implemented dynamics behavior of a linearly tapered circular Timoshenko beam formulation by numerical integration method to reduce the system bandwidth, system degree of freedom without a significant loss of accuracy and verify the gyroscopic effects of shafts rotation in rotor dynamic. Zorzi et al. [6] investigated the effect of constant axial torque on the dynamics, reliability, safety and survivability of rotor-bearing systems using FEM and determine the static bulking torque and critical speeds of long and short bearing. By using Bernoulli-Euler beam theory, Bert [7] developed governing equation of composite shaft, including effect of gyroscopic, bending and torsion coupling and determines critical speeds of composite shaft. Kim and Bert [8] adopted Sanders best first approximation shell theory to determine critical speeds of a rotating circular cylinder hollow shaft, containing layers of arbitrary laminated composite material. Abramovich et al. [9] employed a special orthogonality procedure which is applied to help understanding the dynamic behavior of the non-symmetrical laminated beam. Further by using Bresse-Timoshenko beam theory, Bert and Kim [10] employed Hamilton's principle to derive equations of motion of composite shafts and to find out critical speeds. Bert and Kim [11] analyzed the dynamic instability of a composite drive shaft subjected to fluctuating torque and/ or rotational speed by using various shell theories and they investigated effect of constant torque and rotational speed. Singh and Gupta [12] implemented a Layer wise Beam Theory (LBT) with assuming a layer-wise

displacement field and were extended to solve a composite rotor dynamic problem. Again Singh and Gupta [13] analyzed and compared the conventional rotor dynamic parameter like natural frequencies, critical speeds, damping factor, unbalance response (UBR) and threshold stability by using EMBT and LBT. Forrai [14] implemented a finite element model for stability analysis of self-excited bending vibrations of linear symmetrical rotor bearing system with internal damping. Chatelet et al. [15] proposed a finite element modeling to reduce the dynamic behavior of rotating structures and whole disk shaft assembly is supposed to be cyclically symmetrically. By using FOSD beam theory (continuum based Timoshenko beam theory), M. Y. Chang et al. [16] implemented the vibration behaviors of rotating laminated composite shaft model where transverse shear deformation, rotary inertia, gyroscopic effects and coupling effect are incorporated. Kapuria et al. [17] presents static and dynamic electro-thermo-mechanical analysis of angle-ply hybrid piezoelectric beams using an efficient coupled zigzag theory. Span-to-thickness ratio, type of loading and the orientation of the angle-ply on the accuracy of the theories is investigated. Gubran et al. [18] analyzed natural frequencies of composite tubular shafts by using modified EMBT with shear deformation, rotary inertia and gyroscopic effects. Modifications take into account effects of stacking sequence and different coupling mechanisms in composite materials. By using FEM, Wang et al. [19] established a solution method for the one-dimensional transient temperature and thermal stress fields in non-homogeneous materials. Syed et al. [20] investigated simple analytical expressions for computing thermal stresses in fiber-reinforced composite beams with rectangular and hat sections due to change of temperature. By using a homogenized finite element beam model, Sino et al. [21] analyzed dynamic instability and natural frequencies of an internally damped rotating composite shaft. The influence of laminate parameters: stacking sequences, fiber orientation, transversal shear effect on natural frequencies and instability thresholds of the shaft are considered.

2.3 Functionally Graded Materials Structure

Feldman and Aboudi [22] studied the elastic bifurcational buckling of FG plates under in-plane compressive load. They concluded that with optimal non-uniform distribution of reinforcing phases, the buckling load can be significantly improved for FG plate over the plate with uniformly distributed reinforcing phase. Praveen and Reddy [23] investigated static and dynamic response of the FG ceramic-metal plates using a simple power law distribution and a finite element that accounted for the transverse shear strains, rotary inertia and moderately large rotations in the von- Karman sense. Gasik [24] developed an efficient micromechanical model for computing thermal stresses; evaluating dynamic stress/strain distribution and inelastic behavior of FGMs with an arbitrary non-linear 3D-distribution phases. Suresh and Mortensen [25] provide an excellent introduction to the fundamentals of FGMs. Aboudi et al. [26] developed a more general higher-order theory for FG materials and illustrated the utility of FG microstructures in tailoring the behavior of structural components in various applications. Nakamura et al. [27] investigated Kalman filter technique which was originally introduced for signal/digital filter processing, is used to estimate FGM through-thickness compositional variation and a rule-of-mixtures parameter that defines effective properties of FGMs. Wang et al. [28] proposed a method to determine the transient and

steady state thermal stress intensity factors of graded composite plate containing non-collinear cracks subjected to dynamic thermal loading. Woo and Meguid [29] presented an analytical solution for the large deflections of plates and shallow shells made of FGMs under the combined action of thermal and mechanical loads. Sankar [30] provided an elasticity solution for FG beams in which the beam properties are graded in the thickness direction according to an exponential law. Here FG Euler-Bernoulli beam theory considered under mechanical loading. Sankar and Tzeng [31] expanded upon Sankar's [30] earlier work by investigating beams with through the thickness temperature gradients. Chakraborty et al. [32] proposed a two-node beam element for FGMs based on FOSD theory and applied it to static, thermal, free vibration and wave propagation problems. They assumed displacement field of the element satisfies the general solution to the static part of the governing equations. Nemta AIIa [33] introduced 2D-FGM, for withstand super high temperatures and to give more reduction in thermal stresses. Reddy [34] worked on characterizing the theoretical formulation of FGMs to include the derivations of equations used to calculate material properties throughout the thickness of the material based on the through-the-thickness distribution of materials. Na and Kim [35] studied the thermo-mechanical buckling of FGMs using a finite element discretization method. Przybyowicz [36] presented a problem of active stabilization of a rotating shaft made of a three-phase FG Material with piezoelectric fraction and determination of such a distribution of the volume fraction of the active phase within the shaft, which makes the system possibly most resistant to self-excitation. Cooley [37] researched FGM shell panels under thermal loading using the FEM. By using a multi-layered approach, Shao [38] analyzed the analytic solutions of temperature, displacements, and thermal/mechanical stresses in a FG circular hollow cylinder. Based on the FOSD theory and von-Karman nonlinear kinematics, WU et al. [39] obtained a solution for the nonlinear static and dynamic responses of the FG materials rectangular plate. Argeso and Eraslan [40] developed a computational model for the analysis of elastic, partially plastic and residual stress states in long FG rotating solid shafts. Rahimi and Davoodinik [41] developed the analysis of thermal behavior and distribution of material properties of FG beam. For thermal loading the steady state of heat conduction with exponentially and hyperbolic variations through the thickness of FGB, is considered. Piovan and Sampaio [42] developed a rotating nonlinear FG beam model accounting for arbitrary axial deformations. This model is also employed to analyze other simplified models based on isotropic materials or composite materials. By using first-order shear deformation plate theory Zhao et al. [43] presented the mechanical and thermal buckling analysis of FG ceramic–metal plates. By using Ritz method and HOSD beam theories, Simsek [44] investigated Static analysis of a FG Timoshenko simply-supported beam subjected to a uniformly distributed load. By using Classical beam theories Giunta et al. [45] analyzed linear static analysis of beams made of materials whose properties are graded along one or two directions. Afsar and Go [46] developed the finite element analysis of thermo-elastic field in a thin circular FGM disk subjected to a thermal load and an inertia force due to rotation of the disk. By using different higher-order beam theories, Simsek [47] analyzed fundamental frequency of FG beams having different boundary conditions. Alibeigloo [48] developed analytical solution for FGM beams integrated with piezoelectric actuator and sensor under an applied electric field and thermo-mechanical load. Kocaturk et al. [49]

studied non-linear static analysis of a cantilever Timoshenko beam composed of FGM under a non-follower transversal uniformly distributed load with large displacements and large rotations. Mazzei and Scott [50] investigated the FGMs on resonance of bending shafts under time-dependent axial loading. By differential quadrature method, Alashti and Khorsand [51] carried out three-dimensional thermo- elastic analysis of a FG cylindrical shell with piezoelectric layers under the effect of asymmetric thermo- electro-mechanical loads.

2.4 Vibration and Control

Dimentberg [52] studied both viscous and hysteretic internal damping and listed that viscous damping is destabilizing at speeds beyond the first critical, hysteretic damping is destabilizing at all speeds. Gunter and Trumpler [53] studied the influence of internal friction on the stability of high speed rotors with anisotropic supports. Ruhl [54], Ruhl and Booker [55] described a FEM for modeling a rotor-system only including translational inertia and bending effects. Lund [56] analyzed stability of damped critical speeds of a flexible rotor supported by identical fluid film bearings. Dimarogonas [57] devised a general method for stability analysis of rotating shafts including rotary inertia, gyroscopic effect and internal damping with a combination of a transfer matrix technique. Zorzi and Nelson [58] developed a FE simulation of rotor-bearing systems with considering internal damping (viz. viscous and hysteretic damping) effects. Dutt and Nakra [59] founded that viscoelastic supports increase the stability limit compared to that with either viscously damped flexible supports or elastic supports. Abduljabbar et al. [60] addressed an active vibration controller for controlling the dynamics of a flexible rotor running in flexibly-mounted journal bearings. Wettergren et al. [61] analyzed that instability can be avoided or minimized with appropriate selection of external damping, asymmetry in shaft stiffness and non-isotropic force coefficients. Qin and Mao [62] developed a new shaft element model with ten DOF for coupled torsional-flexural vibration of rotor systems including the effects of translational and rotational inertia, gyroscopic moments, bending, shear and torsional deformations, internal damping, and mass eccentricity. Dutt and Nakra [63] used a popular minimization technique to reduce rotor vibration by applying viscoelastic bearing supports. Ku [64] formulated a C^0 class Timoshenko beam FE model to analyze the dynamic characteristics of a rotor bearing system with hysteretic internal damping. By using Mori-Tanaka mean field theory, M. Y. Chang et al. [65] implemented the vibration analysis of rotating composite shafts containing randomly oriented reinforcement. They investigated the natural frequency of stationary shafts and whirling speeds as well as critical speeds of rotating shafts. Roy et al. [66] proposed an augmenting thermodynamic field (ATF) technique for theoretical study of the dynamics of a viscoelastic rotor-shaft system containing that internal material damping. By using TBT, Xiang et al. [67] analyzed free and forced vibration of a laminated FG beam of variable thickness under thermally induced initial stresses and both the axial and rotary inertia of the beam are considered. The beam consists of a homogeneous substrate and two inhomogeneous FG layers whose material composition follows a power law distribution in the thickness direction in terms of the volume fractions of the material constituents. Based on the three-dimensional linear elasticity theory, Li et al. [68] analyzed free vibration of FG material sandwich rectangular plates with simply supported and clamped edges. Das et al.

[69] proposed an active vibration control scheme for controlling transverse vibration of a rotor shaft due to unbalance forces and theoretical study. Using Bernoulli-Euler beam theory (BEBT) and the rotational spring model, free vibration and buckling response of FG beams with edge cracks were considered by Yang and Chen [70]. Based on TBT, Ke et al. [71] studied free vibration and elastic buckling of beams made of FGMs containing open edge cracks. It is assumed that the material properties follow exponential distributions along beam thickness direction. By using multiple scales method, Hosseini et al. [72] studied free vibrations of an in-extensional simply supported rotating shaft with nonlinear curvature and inertia. Rotary inertia and gyroscopic effects are included, but shear deformation is neglected. Boyaci et al. [73] investigated critical bifurcations emanating destructive limit-cycle oscillations of higher amplitudes and the influence of the shaft elasticity on the critical limit-cycle oscillations. By using HOSD, Mahi et al. [74] studied exact solutions of the free vibration of a beam made of symmetric FG materials. Here material properties are taken to be temperature-dependent and vary continuously through the thickness according to a power law distribution (P-FGM), or an exponential law distribution (E-FGM) or a sigmoid law distribution (S-FGM). By using boundary element method (BEM), Sapountzakis et al. [75] developed a general flexural-torsional vibration problem of Timoshenko beams of arbitrarily shaped composite cross-section taking into account the effects of warping stiffness, warping and rotary inertia and shear deformation. Boukhalfa and Hadjoui [76] employed hp -version, hierarchical finite element model and concerned with the dynamic behavior of the rotating composite shaft on rigid bearings. Thermal buckling behaviour of FG beams associated with different boundary conditions were investigated by Kiani and Eslami [77] by using the EBBT. Shahba et al. [78] developed free vibration and stability analysis of axially FG homogeneous tapered Timoshenko beams through a finite element approach. By using EBBT, Alshorbagy et al. [79] presented the dynamic characteristics of FG beam by FEM with material graduation in axially or transversally through the thickness based on the power law. By EBBT and von Karman geometric nonlinearity, Rafiee et al. [80] investigated effects of material property distribution on the nonlinear dynamic behavior of FG beams and effects of different parameters on the frequency-response. Kumar et al. [81] developed analytical solution for the free vibration analysis of FGM plate without enforcing zero transverse shear stress conditions on the top and bottom surfaces of the plate using higher order displacement model.

2.5 Motivation

Although literature review reveals that a lot of research work has been done on vibration analysis of composite and functionally graded structures. The studies on the analysis of vibration and stability of rotor shaft system with FGMs based on the Timoshenko beam under thermo-mechanical loading yet have not been discussed. This present work will explore vibration and stability analyses of functionally graded rotating shaft system based on finite element method under thermal environment. FGM performance is first characterized under thermal environments and mechanical loading in order to understand the unique characteristics of FGMs and to compare FGM structural response to traditional metal structure. The main advantage of using FGMs instead of traditional materials is that the

internal composition of their component materials can be tailored to satisfy the requirements of a particular structure. Although this technology has not fully implemented so internal structure of the material could be prepared to manufacture pressure vessels and other thermal structure. This work is an important step in being able to properly design mechanical structure using a FGMs system. The core portion of structure is made FGMs could resist high temperature and mass, structure size requirements can be reduced by tailoring the ingredient of each component based upon load and stress interaction in different areas of mechanical structure. FGMs are of increasing importance as designers seek a way to address structure under combined mechanical and thermal loads. The finite element method is commonly employed to analyze structure like beam, plate, shell and solid elements. But for FGMs it is important step to achieve this goal, a first order shear deformation (FOSD) FG shaft model is formulated and applied to shaft subjected to temperatures and mechanical loading.

2.6 Objectives of Present Work

The specific objectives of the present thesis have been laid down as

- Development of material modeling for FG shaft based on the different laws of gradation
- Modeling of FG shaft with temperature dependent material properties
- Effects of different temperatures and power law gradient indexes on variation of mechanical properties through the radial direction of the FG shaft.
- Finite modeling of FG spinning shaft system (i.e. rotor-bearing-shaft system) in order to study the vibration behavior of this shaft system
- To study the vibration and stability analysis of FG shaft system by incorporating internal viscous and hysteretic damping
- To comparative study of the various responses of FG shaft over steel shaft
- To study the effects of different temperatures and power law gradient indexes on the various responses of the FG shaft.
- To study the dynamic behaviors (i.e. critical speed, fundamental frequencies, Campbell diagram, Damping ratio, Time response and Stability Limit Speed) of rotating FG shaft system under thermal and mechanical loadings by incorporating internal viscous and hysteretic damping

CHAPTER 3

MODELING FOR EFFECTIVE MATERIALS PROPERTIES OF FG SHAFT

This chapter modeling of FG material to obtain the effective material properties of FG shaft by considering power law gradation and exponential law gradation.

3.1 Effective Materials Properties of FGM

As FGMs are heterogeneous materials so there is need for the determination of effective material properties. To achieve best performance, accurate material property estimation is essential for analysis and design of FG structures/system. There are various models developed to determine the material properties of FGM such as

1) Rules of mixtures: Linear rule of mixtures and Harmonic rule of mixtures
2) Variational approach
3) Micromechanical approaches

Rules of mixtures employ bulk constituent properties assuming no interaction between phases. This approach derived from continuum mechanics and is free from empirical considerations. In variational approach, variational principles of thermo-mechanics used to derive the bounds for effective thermo-physical properties. Micromechanical approaches include information about spatial distribution of the constituent materials. Standard micromechanical approach is based on concept of unit cell or representative volume element (RVE) to represent the microstructure of composite.

3.2 Modeling for Material Properties of FG Rectangular Cross-section

A FGM beam is considered having with finite length *L* and Thickness *t* and also made of a mixture of ceramics (aluminum oxide) and metal (stainless steel). Here material in top surface $\left(z=\frac{t}{2}\right)$ and in bottom surface $\left(z=-\frac{t}{2}\right)$ of the shaft is ceramic and metal respectively. The effective material properties P can be written as,

$$P = P_c V_c + P_m V_m \tag{1}$$

Where, P_c and P_m are the material properties of the ceramic and metal respectively. Now V_c and V_m are the volume fractions of ceramic and metal respectively and they are related by,

$$V_c + V_m = 1 \tag{2}$$

3.2.1 Power Law Gradation

In Fig. 3.1 V_c describes the volume fraction of ceramic at any point z throughout the thickness t according to volume fraction index n which controls the shape of the function and variation is assumed to be in terms of a simple power law. The power law is expressed by,

$$V_c(z) = \left(\frac{2z+t}{2t}\right)^k \tag{3}$$

Where k is the volume fraction index ($k \geq 0$).

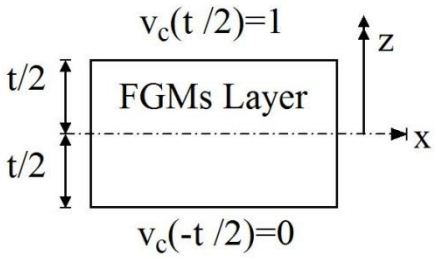

Fig. 3.1 Volume fraction of ceramic throughout the FGM layer

The material properties P that are temperature dependent can be written as,

$$P = P_0(P_{-1}T^{-1} + 1 + P_1T + P_2T^2 + P_3T^3) \tag{4}$$

Where P_{-1}, P_1, P_2 and P_3 are the coefficient of temperature T^{-1}, T, T^2 and T^3 respectively. From equation (1) to (4), the modulus of elasticity(E), Poisson's ratio(ν), coefficient of thermal expansion(α), thermal conductivity (K) and the density(ρ) are written as,

$$\begin{aligned}
E(z,T) &= \{E_c(T) - E_m(T)\}\left(\frac{2z+t}{2t}\right)^k + E_m(T) \\
\nu(z,T) &= \{\nu_c(T) - \nu_m(T)\}\left(\frac{2z+t}{2t}\right)^k + \nu_m(T) \\
\alpha(z,T) &= \{\alpha_c(T) - \alpha_m(T)\}\left(\frac{2z+t}{2t}\right)^k + \alpha_m(T) \\
K(z,T) &= \{K_c(T) - K_m(T)\}\left(\frac{2z+t}{2t}\right)^k + K_m(T) \\
\rho(z) &= (\rho_c - \rho_m)\left(\frac{2z+t}{2t}\right)^k + \rho_m
\end{aligned} \tag{5}$$

Here only density(ρ) is assumed to be a constant and only it is vary along radial position and power law gradient index and independent of temperature.

3.2.2 Exponential Gradation Law

In exponential gradation the materials properties are assume to vary according to

$$P(z) = P_0 e^{k\left(z+\frac{t}{2}\right)} \tag{6}$$

Where P_0 refers the material properties of bottom surface of the FGM shaft and ' k ' is the parameter describing the gradation across the thickness direction. Now modulus of elasticity, coefficient of thermal expansion, thermal conductivity and density of the FGM shaft varies as,

$$\begin{aligned} E(z) &= E_0 e^{k\left(z+\frac{t}{2}\right)}, \alpha(z) = \alpha_0 e^{k\left(z+\frac{t}{2}\right)} \\ K(z) &= K_0 e^{k\left(z+\frac{t}{2}\right)}, \rho(z) = \rho_0 e^{k\left(z+\frac{t}{2}\right)} \end{aligned} \tag{7}$$

Here Poisson ratio assumed as constant. This law reflects the simple rule of mixtures used to obtain properties of FGM shaft and computational effort is to be reduced.

3.3 Modeling for Material Properties of FG Circular Cross-section

A FGM shaft is considered with finite length *L*, inner radius (r_i) and outer radius (r_o). Material of the shaft is considered in top surface $(z = r_i/2)$ as ceramic and in bottom surface $(z = r_o/2)$ as metal.

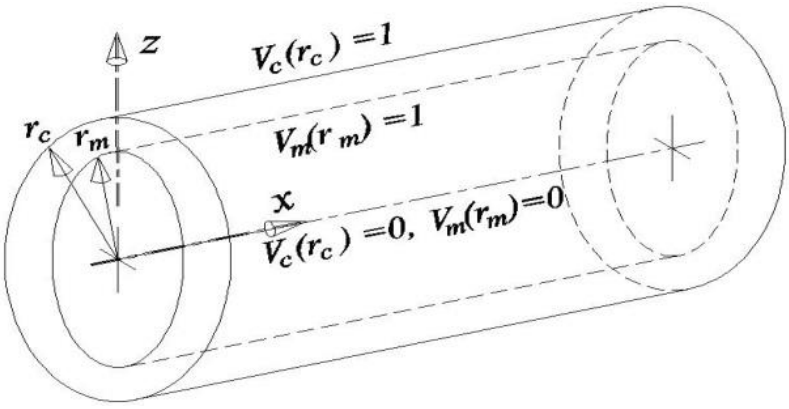

Fig. 3.2 Volume fraction of ceramic and metal throughout the FGM layer

3.3.1 Power Law Gradation

In Fig. 3.2, V_c and V_m describes the volume fraction of ceramic and metal respectively at any point *z* throughout the radius *r* according to power law and power law gradient index (k) controls the shape of the function. The power law is expressed by,

$$V_m(z)=\left(\frac{r-r_m}{r_c-r_m}\right)^k \tag{8}$$

Where power law gradient index is considered greater than and equal to zero i.e. $k \geq 0$

Now according to power law distribution variations of temperature dependent material properties (Young's modulus(E), Poisson's ratio(ν), Coefficient of thermal expansion (α) and Thermal conductivity(K)) along radial direction of FG circular shaft becomes,

$$\begin{aligned}
E(z,T)&=\left\{E_c(T)-E_m(T)\right\}\left(\frac{r-r_m}{r_c-r_m}\right)^k+E_m(T)\\
\nu(z,T)&=\left\{\nu_c(T)-\nu_m(T)\right\}\left(\frac{r-r_m}{r_c-r_m}\right)^k+\nu_m(T)\\
\alpha(z,T)&=\left\{\alpha_c(T)-\alpha_m(T)\right\}\left(\frac{r-r_m}{r_c-r_m}\right)^k+\alpha_m(T)\\
K(z,T)&=\left\{K_c(T)-K_m(T)\right\}\left(\frac{r-r_m}{r_c-r_m}\right)^k+K_m(T)\\
\rho(z)&=\left(\rho_c-\rho_m\right)\left(\frac{r-r_m}{r_c-r_m}\right)^k+\rho_m
\end{aligned} \tag{9}$$

Here only density(ρ) is assumed to be a constant and only it is vary along radial position and power law gradient index.

Now, nonlinear temperature distribution (NLTD) is assumed to occur in the radial direction of FG shaft where the temperature T_c and T_m are in ceramic-rich and metal-rich surfaces respectively. In the absence of heat generation, the temperature field for the steady-state one dimensional Fourier equation of heat conduction law becomes as,

$$\frac{d}{dz}\left[K(z)\frac{dT}{dz}\right]=0 \tag{10}$$

Where, at $z=(r_i/2)$, $T=T_{top}$ and at $z=(r_o/2), T=T_{bottom}$ Now the solution of equation obtained by polynomial series and written by,

$$T(z)=T_m+(T_c-T_m)\zeta(z) \tag{11}$$

Where,

$$\zeta(z)=\frac{1}{C}\left[\left(\frac{r-r_m}{r_c-r_m}\right)-\frac{K_{cm}}{(k+1)K_m}\left(\frac{r-r_m}{r_c-r_m}\right)^{k+1}+\frac{K_{cm}^2}{(2k+1)K_m^2}\left(\frac{r-r_m}{r_c-r_m}\right)^{2k+1}-\frac{K_{cm}^3}{(3k+1)K_m^3}\left(\frac{r-r_m}{r_c-r_m}\right)^{3k+1}\right.$$
$$\left.+\frac{K_{cm}^4}{(4k+1)K_m^4}\left(\frac{r-r_m}{r_c-r_m}\right)^{4k+1}-\frac{K_{cm}^5}{(5k+1)K_m^5}\left(\frac{r-r_m}{r_c-r_m}\right)^{5k+1}\right]$$

$$C=1-\frac{K_{cm}}{(k+1)K_m}+\frac{K_{cm}^2}{(2k+1)K_m^2}-\frac{K_{cm}^3}{(3k+1)K_m^3}+\frac{K_{cm}^4}{(4k+1)K_m^4}-\frac{K_{cm}^5}{(5k+1)K_m^5}$$

$$K_{cm}=K_c-K_m.$$

CHAPTER 4

FORMULATION FOR GOVERNING EQUATIONS OF ROTOR SHAFT SYSTEM

4.1 Introduction

Based on the FOSD theory, shaft is modeled as a Timoshenko beam with considering rotary inertia and gyroscopic effect. The shaft is considered uniform circular cross-section and it is rotate at constant speed about its longitudinal axis. The displacements variables and schematic diagram of rotor-bearing system are shown with coordinate systems in Fig. 4.1 and Fig. 4.2 respectively.

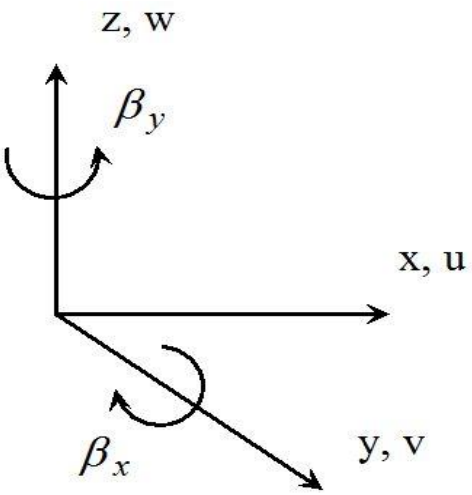

Fig. 4.1 Displacement and rotational variables with coordinate systems

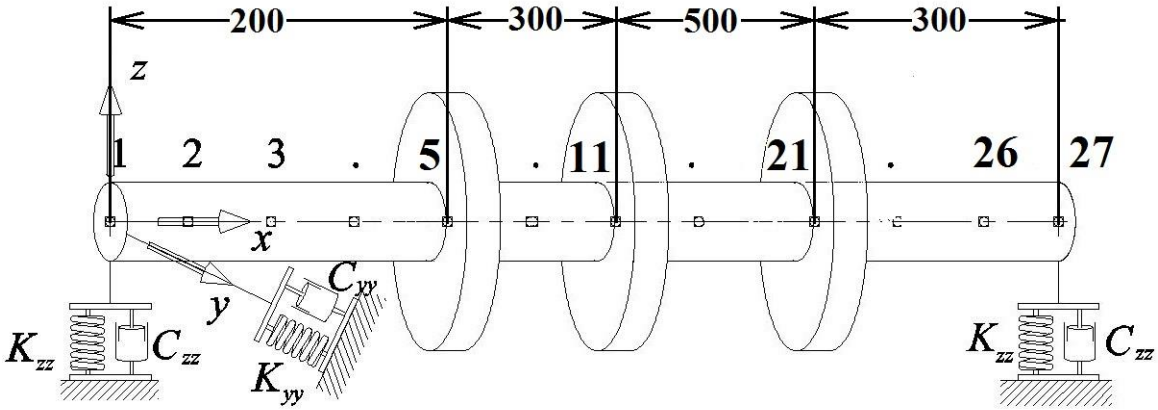

Fig. 4.2 Schematic diagram of rotor-bearing system with coordinate systems

4.2 Mathematical Modeling of Functionally Graded Shaft

The displacement fields are assumed as follow

$$\begin{aligned} u_x(x,y,z,t) &= z\beta_x(x,t) - y\beta_y(x,t) \\ v_y(x,y,z,t) &= v_0(x,t) \\ w_z(x,y,z,t) &= w_0(x,t) \end{aligned} \tag{12}$$

where u_x , v_x and w_x are the flexural displacements of any point on the cross-section of the shaft in the x , y and z directions , the variables v_0 and w_0 are the flexural displacements of the shaft's axis, while β_x and β_y are the rotation angles of the cross-section , about the y and z axis, respectively. Now strain components in the cylindrical system can be written in terms of the displacement variables as follow,

$$\begin{aligned} \varepsilon_{xx} &= \frac{\partial u}{\partial x} \\ \varepsilon_{x\theta} &= \frac{1}{2}\left(\frac{1}{r}\frac{\partial u}{\partial x} + \cos\theta\frac{\partial v}{\partial x} - \sin\theta\frac{\partial w}{\partial x}\right) \\ \varepsilon_{xr} &= \frac{1}{2}\left(\frac{u}{r} + \cos\theta\frac{\partial v}{\partial x} + \sin\theta\frac{\partial w}{\partial x}\right) \end{aligned} \tag{13}$$

After simplifying,

$$\begin{aligned} \varepsilon_{xx} &= r\sin\theta\frac{\partial \beta_x}{\partial x} - r\cos\theta\frac{\partial \beta_y}{\partial x} \\ \varepsilon_{rr} &= \varepsilon_{\theta\theta} = \varepsilon_{r\theta} = 0 \\ \varepsilon_{xr} &= \varepsilon_{rx} = \frac{1}{2}\left(\beta_x\sin\theta - \beta_y\cos\theta + \sin\theta\frac{\partial w_0}{\partial x} + \cos\theta\frac{\partial v_0}{\partial x}\right) \\ \varepsilon_{x\theta} &= \varepsilon_{\theta x} = \frac{1}{2}\left(\beta_y\sin\theta + \beta_x\cos\theta - \sin\theta\frac{\partial v_0}{\partial x} + \cos\theta\frac{\partial w_0}{\partial x}\right) \end{aligned} \tag{14}$$

Now the strain terms can be represents in matrix form as,

$$\begin{bmatrix} \varepsilon_{xx} \\ \gamma_{x\theta} \\ \gamma_{xr} \end{bmatrix} = \begin{bmatrix} 0 & 0 & r\sin\theta\dfrac{\partial}{\partial x} & -r\cos\theta\dfrac{\partial}{\partial x} \\ -\sin\theta\dfrac{\partial}{\partial x} & \cos\theta\dfrac{\partial}{\partial x} & \cos\theta & \sin\theta \\ \cos\theta\dfrac{\partial}{\partial x} & \sin\theta\dfrac{\partial}{\partial x} & \sin\theta & -\cos\theta \end{bmatrix} \begin{bmatrix} v_0 \\ w_0 \\ \beta_x \\ \beta_y \end{bmatrix} \tag{15}$$

The stress–strain relations of the r^{th} layer expressed in the cylindrical coordinate system can be expressed as

$$\begin{aligned}\sigma_{xx} &= \overline{C}_{11\mathrm{r}}\varepsilon_{xx} + k_s\overline{C}_{16\mathrm{r}}\gamma_{x\theta}\\ \tau_{x\theta} &= \tau_{\theta x} = k_s\overline{C}_{16\mathrm{r}}\varepsilon_{xx} + k_s\overline{C}_{66\mathrm{r}}\gamma_{x\theta}\\ \tau_{xr} &= \tau_{rx} = k_s\overline{C}_{55\mathrm{r}}\gamma_{xr}\end{aligned} \tag{16}$$

In matrix form stress-strain relations of r^{th} layer expressed in the cylindrical coordinate system can be expressed as

$$\begin{bmatrix}\sigma_{xx}\\ \tau_{x\theta}\\ \tau_{xr}\end{bmatrix} = \begin{bmatrix}\overline{C}_{11\mathrm{r}} & k_s\overline{C}_{16\mathrm{r}} & 0\\ k_s\overline{C}_{16\mathrm{r}} & k_s\overline{C}_{66\mathrm{r}} & 0\\ 0 & 0 & k_s\overline{C}_{55\mathrm{r}}\end{bmatrix}\begin{bmatrix}\varepsilon_{xx}\\ \gamma_{x\theta}\\ \gamma_{xr}\end{bmatrix} \tag{17}$$

Stress-strain relation matrix,

$$D = \begin{bmatrix}\overline{C}_{11\mathrm{r}} & k_s\overline{C}_{16\mathrm{r}} & 0\\ k_s\overline{C}_{16\mathrm{r}} & k_s\overline{C}_{66\mathrm{r}} & 0\\ 0 & 0 & k_s\overline{C}_{55\mathrm{r}}\end{bmatrix}$$

Where k_s the shear correction factor and $\overline{C}_{ijr}$ is the constitutive matrix which is related to elastic constants of principle axes.

4.3 Strain Energy Expression for FG Shaft

Now Strain energy expression of FG shaft can be obtains as follows,

$$U_s = \frac{1}{2}\int_V [\sigma]^T[\varepsilon]dV = \frac{1}{2}\int_V (\sigma_{xx}\varepsilon_{xx} + \sigma_{rr}\varepsilon_{rr} + \sigma_{\theta\theta}\varepsilon_{\theta\theta} + 2\tau_{xr}\varepsilon_{xr} + 2\tau_{x\theta}\varepsilon_{x\theta} + 2\tau_{r\theta}\varepsilon_{r\theta})dV$$

$$\because \varepsilon_{rr} = \varepsilon_{\theta\theta} = \varepsilon_{r\theta} = 0$$

So strain energy expression can be rewritten as

$$U_s = \frac{1}{2}\int_V (\sigma_{xx}\varepsilon_{xx} + 2\tau_{xr}\varepsilon_{xr} + 2\tau_{x\theta}\varepsilon_{x\theta})dV \tag{18}$$

Where total volume of the element $\mathrm{V} = (rd\theta dxdr)$

Now,

$$\int_V (\sigma_{xx}\varepsilon_{xx})dV = \int_V (\overline{C}_{11n}\varepsilon_{xx} + k_s\overline{C}_{16n}\gamma_{x\theta})\varepsilon_{xx}dV = \int_V (\overline{C}_{11n}\varepsilon_{xx}{}^2 + k_s\overline{C}_{16n}\gamma_{x\theta}\varepsilon_{xx})dV$$

$$= B_{11}\left[\int_0^L\left(\frac{\partial\beta_x}{\partial x}\right)^2 dx + \int_0^L\left(\frac{\partial\beta_y}{\partial x}\right)^2 dx\right] + \frac{1}{2}k_s A_{16}\left[\left(\int_0^L \beta_y\frac{\partial\beta_x}{\partial x}dx\right) - \left(\int_0^L \beta_x\frac{\partial\beta_y}{\partial x}dx\right) - \left(\int_0^L \frac{\partial v_0}{\partial x}\frac{\partial\beta_x}{\partial x}dx\right) - \left(\int_0^L \frac{\partial w_0}{\partial x}\frac{\partial\beta_y}{\partial x}dx\right)\right]$$

$$\int_V (2\tau_{xr}\varepsilon_{xr})dV = \int_V (2k_s\overline{C}_{55n}\gamma_{xr})\varepsilon_{xr}dV = \int_V k_s\overline{C}_{55n}(\varepsilon_{xr})^2 dV$$

$$= k_s A_{55}\left[\int_0^L \beta_x^2 dx + \int_0^L \beta_y^2 dx + \int_0^L\left(\frac{\partial v_0}{\partial x}\right)^2 dx + \int_0^L\left(\frac{\partial w_0}{\partial x}\right)^2 dx - \left(2\int_0^L \beta_y\frac{\partial v_0}{\partial x}dx\right) + \left(2\int_0^L \beta_x\frac{\partial w_0}{\partial x}dx\right)\right]$$

$$\int_V (2\tau_{x\theta}\varepsilon_{x\theta})dV = \int_V 2(k_s\overline{C}_{16n}\varepsilon_{xx} + k_s\overline{C}_{66n}\gamma_{x\theta})\varepsilon_{x\theta}dV$$

$$= \left[\begin{array}{l} \frac{1}{2}k_s A_{16}\left\{\left(\int_0^L \beta_y\frac{\partial\beta_x}{\partial x}dx\right) - \left(\int_0^L \beta_x\frac{\partial\beta_y}{\partial x}dx\right) - \left(\int_0^L \frac{\partial v_0}{\partial x}\frac{\partial\beta_x}{\partial x}dx\right) - \left(\int_0^L \frac{\partial w_0}{\partial x}\frac{\partial\beta_y}{\partial x}dx\right)\right\} \\ +k_s A_{66}\left\{\int_0^L \beta_x^2 dx + \int_0^L \beta_y^2 dx + \int_0^L\left(\frac{\partial v_0}{\partial x}\right)^2 dx + \int_0^L\left(\frac{\partial w_0}{\partial x}\right)^2 dx + \left(2\int_0^L \beta_x\frac{\partial w_0}{\partial x}dx\right) - \left(2\int_0^L \beta_y\frac{\partial v_0}{\partial x}dx\right)\right\} \end{array}\right]$$

Now taking first variation of above strain energy expression and obtains,

$$\delta U_S = \left[\begin{array}{l} B_{11}\left[\begin{array}{l} \int_0^L\left(\frac{\partial\beta_x}{\partial x}\frac{\partial\delta\beta_x}{\partial x}\right)dx \\ +\int_0^L\left(\frac{\partial\beta_y}{\partial x}\frac{\partial\delta\beta_y}{\partial x}\right)dx \end{array}\right] + \frac{1}{2}k_s A_{16}\left[\begin{array}{l} \int_0^L\left(\beta_y\frac{\partial\delta\beta_x}{\partial x} + \frac{\partial\beta_x}{\partial x}\delta\beta_y\right)dx - \int_0^L\left(\beta_x\frac{\partial\delta\beta_y}{\partial x} + \frac{\partial\beta_y}{\partial x}\delta\beta_x\right)dx \\ -\int_0^L\left(\frac{\partial v_0}{\partial x}\frac{\partial\delta\beta_x}{\partial x} + \frac{\partial\beta_x}{\partial x}\frac{\partial\delta v_0}{\partial x}\right)dx - \int_0^L\left(\frac{\partial w_0}{\partial x}\frac{\partial\delta\beta_y}{\partial x} + \frac{\partial\beta_y}{\partial x}\frac{\partial\delta w_0}{\partial x}\right)dx \end{array}\right] \\ +k_s\left(A_{55}+A_{66}\right)\left[\begin{array}{l} \int_0^L \beta_x\delta\beta_x dx + \int_0^L \beta_y\delta\beta_y dx + \int_0^L\left(\frac{\partial v_0}{\partial x}\frac{\partial\delta v_0}{\partial x}\right)dx \\ +\int_0^L\left(\frac{\partial w_0}{\partial x}\frac{\partial\delta w_0}{\partial x}\right)dx - \int_0^L\left(\beta_y\frac{\partial\delta v_0}{\partial x} + \frac{\partial v_0}{\partial x}\delta\beta_y\right)dx + \int_0^L\left(\beta_x\frac{\partial\delta w_0}{\partial x} + \frac{\partial w_0}{\partial x}\delta\beta_x\right)dx \end{array}\right] \end{array}\right] \quad (19)$$

The terms A_{16}, A_{55}, A_{66} and B_{11} are given in Appendix.

4.4 Kinetic Energy Expression for FG Shaft

The kinetic energy of the rotating composite shaft including the effects of translatory and rotary can be written as follow,

$$T_s = \frac{1}{2}\int_0^L\left[\mathrm{I_m}(\dot{v_0}^2 + \dot{w_0}^2) + I_d(\dot{\beta_x}^2 + \dot{\beta_y}^2) - 2\Omega I_p\beta_x\dot{\beta_y}^2 + \Omega^2 I_d(\beta_x{}^2 + \beta_y{}^2) + \Omega^2 I_p\right]dx \quad (20)$$

Where Ω is the rotating speed of the shaft which is assumed constant, L is the total length of the shaft, the gyroscopic effect denotes by $2\Omega \mathrm{I}_P \beta_x \dot{\beta}_y$ and rotary inertia effect is representing by $I_d\left(\dot{\beta}_x^2+\dot{\beta}_y^2\right)$. The mass moment of inertia denotes by I_m and the diametrical mass moments of inertia represent by I_d and polar mass moment of inertia I_p of rotating shaft per unit length is defined in the appendix. As the term $\Omega^2 I_d\left(\beta_x^2+\beta_y^2\right)$ is far smaller than $\Omega^2 I_p$ so it will neglect in further analysis. The terms I_m, I_d and I_p are given in appendix.

Now taking first variation of the kinetic energy of shaft obtains as,

$$\delta T_s=\int_0^L\left[\begin{array}{l}\mathrm{I_m}\left(\dot{v}_0\dfrac{\partial\delta v_0}{\partial t}+\dot{w}_0\dfrac{\partial\delta w_0}{\partial t}\right)+I_d\left(\dot{\beta}_x\dfrac{\partial\delta\beta_x}{\partial t}+\dot{\beta}_y\dfrac{\partial\delta\beta_y}{\partial t}\right)\\ -\Omega I_p\left(\dot{\beta}_y\,\delta\beta_x+\beta_x\dfrac{\partial\delta\beta_y}{\partial t}\right)\end{array}\right]dx \tag{21}$$

4.5 Kinetic Energy Expression for Disks

Here assumption is made that disks are fixed to the shafts and material of the shafts are considered as isotropic material and kinetic energy expression of the disks can be obtains as ,

$$T_d=\frac{1}{2}\int_0^L\sum_{i=1}^{N_D}\left[\mathrm{I}_{mi}^D\left(\dot{v}_0^2+\dot{w}_0^2\right)+I_{di}^D\left(\dot{\beta}_x^2+\dot{\beta}_y^2\right)-2\Omega I_{pi}^D\beta_x\dot{\beta}_y^2+\Omega^2 I_{pi}^D\right]\Delta\left(x-x_{Di}\right)dx \tag{22}$$

Where disks position is denotes by *i(=1,2,3….)* and I_{mi}^D , I_{di}^D and I_{pi}^D are denotes the mass moment of inertia , the diametrical mass moment of inertia and the polar mass moment of inertia respectively. The symbol $\Delta\left(x-x_{Di}\right)$ denotes the one dimensional spatial Dirac delta function and N_D is the number of discrete disks which is attached with shaft and x_{Di} is the location of the disk.

Now taking the first variation of the kinetic energy of the disk, obtains

$$\delta T_d=\int_0^L\sum_{i=1}^{N_D}\left[\begin{array}{l}\mathrm{I}_{mi}^D\left(\dot{v}_0\dfrac{\partial\delta v_0}{\partial t}+\dot{w}_0\dfrac{\partial\delta w_0}{\partial t}\right)+I_{di}^D\left(\dot{\beta}_x\dfrac{\partial\delta\beta_x}{\partial t}+\dot{\beta}_y\dfrac{\partial\delta\beta_y}{\partial t}\right)\\ -\Omega I_{pi}^D\left(\dot{\beta}_y\,\delta\beta_x+\beta_x\dfrac{\partial\delta\beta_y}{\partial t}\right)\end{array}\right]\Delta\left(x-x_{Di}\right)dx \tag{23}$$

4.6 Work done Expression due to External Loads and Bearings

Here R_y, R_z is assumed the external force intensities (force per unit length) which is subjected on the shaft and M_x, M_y is the external torque intensities (moment per unit length), which is distributed along the shaft. Now virtual work-done by the external loads can be represents as follow,

$$\delta W_E = \int_0^L \left(R_y \delta v_0 + R_z \delta w_0 + M_y \delta \beta_y + M_x \delta \beta_x \right) dx \tag{24}$$

Now bearings are modeled by springs and viscous dampers. Virtual work done by springs and dampers can be represents as,

$$\delta W_B = \int_0^L \sum_{i=1}^{N_B} \begin{pmatrix} -K_{yy}^{Bi} v_0 \delta v_0 - K_{zy}^{Bi} v_0 \delta w_0 - K_{yz}^{Bi} w_0 \delta v_0 - K_{zz}^{Bi} w_0 \delta w_0 \\ -C_{yy}^{Bi} \dot{v}_0 \delta \dot{v}_0 - C_{zy}^{Bi} \dot{v}_0 \delta \dot{w}_0 - C_{yz}^{Bi} \dot{w}_0 \delta \dot{v}_0 - C_{zz}^{Bi} \dot{w}_0 \delta \dot{w}_0 \end{pmatrix} \Delta(x - x_{Bi}) dx \tag{25}$$

Where, N_B denotes number of bearings, x_{Bi} denotes the positions of bearings, K^{Bi} denotes the equivalent stiffness of i^{th} bearings, C^{Bi} denotes the equivalent damping coefficient of i^{th} bearings.

4.7 Governing Equations of Rotor-Shaft System

The governing equations of rotor-shaft system can be derived using equation number (19), (21), (23), (24) and (25) and applying Hamilton's principle which is,

$$\int_{t1}^{t2} \left[\delta T - \delta U_s + \delta W_E + \delta W_B \right] dt = 0$$

Since total kinetic energy of the shaft and disks is $T = T_s + T_d$

$$\int_{t1}^{t2} \left[\delta (T_s + T_d) - \delta U_s + \delta W_E + \delta W_B \right] dt = 0$$

Now simplifying arranging the above equation the motion equations obtains as,

$$\delta v_0 : \mathrm{I_m} \frac{\partial^2 v_0}{\partial t^2} + k_s \left(A_{55} + A_{66} \right) \left(\frac{\partial \beta_y}{\partial x} - \frac{\partial^2 v_0}{\partial x^2} \right) + \frac{1}{2} k_s A_{16} \frac{\partial^2 \beta_x}{\partial x^2} + \sum_{i=1}^{N_D} \mathrm{I}_{mi}^D \frac{\partial^2 v_0}{\partial t^2} \Delta \left(x - x_{Di} \right) + P_{v_0}^b = R_y$$

$$\delta w_0 : \mathrm{I_m} \frac{\partial^2 w_0}{\partial t^2} - k_s \left(A_{55} + A_{66} \right) \left(\frac{\partial^2 w_0}{\partial x^2} + \frac{\partial \beta_x}{\partial x} \right) + \frac{1}{2} k_s A_{16} \frac{\partial^2 \beta_y}{\partial x^2} + \sum_{i=1}^{N_D} \mathrm{I}_{mi}^D \frac{\partial^2 w_0}{\partial t^2} \Delta \left(x - x_{Di} \right) + P_{w_0}^b = R_z$$

$$\delta\beta_x : I_d \frac{\partial^2 \beta_x}{\partial t^2} - I_p \Omega \frac{\partial \beta_y}{\partial t} + \frac{1}{2} k_s A_{16} \frac{\partial^2 v_0}{\partial x^2} - B_{11} \frac{\partial^2 \beta_x}{\partial x^2} - k_s \left(A_{55} + A_{66} \right) \left(\frac{\partial w_0}{\partial x} + \beta_x \right)$$
$$+ \sum_{i=1}^{N_D} \left(I_{di}^D \frac{\partial^2 \beta_x}{\partial t^2} - \Omega \mathrm{I}_{pi}^D \frac{\partial \beta_y}{\partial t} \right) \Delta \left(x - x_{Di} \right) = M_x$$
$$\delta\beta_y : I_d \frac{\partial^2 \beta_y}{\partial t^2} - I_p \Omega \frac{\partial \beta_x}{\partial t} + \frac{1}{2} k_s A_{16} \frac{\partial^2 w_0}{\partial x^2} - B_{11} \frac{\partial^2 \beta_y}{\partial x^2} - k_s \left(A_{55} + A_{66} \right) \left(\beta_x - \frac{\partial v_0}{\partial x} \right)$$
$$+ \sum_{i=1}^{N_D} \left(I_{di}^D \frac{\partial^2 \beta_y}{\partial t^2} - \Omega \mathrm{I}_{pi}^D \frac{\partial \beta_x}{\partial t} \right) \Delta \left(x - x_{Di} \right) = M_y$$

4.8 Solution Procedure

Finite element analysis aim is to find out the field variable (displacement) at nodal points by approximate analysis, assuming at any point inside the element basic variable is a function of values at nodal points of the element, this function is called shape function or interpolation function. Now here employing the approximate solution method the governing equations are approximated by a system of ordinary differential equations. In the present finite element model, the three-nodded one-dimensional line elements are consider, each node having four degrees of freedom.

Lagrangian interpolation functions are used to approximate the displacement fields of shaft. The element's nodal degree of freedom at each node is v_0, w_0, β_x and β_y. Now displacement field variable can be represents as,

$$\begin{aligned} v_0 &= \sum_{k=1}^{r} v_0^k(t)\psi_k(\eta), \quad \beta_x = \sum_{k=1}^{r} \beta_x^k(t)\psi_k(\eta) \\ w_0 &= \sum_{k=1}^{r} w_0^k(t)\psi_k(\eta), \quad \beta_y = \sum_{k=1}^{r} \beta_y^k(t)\psi_k(\eta) \end{aligned} \tag{26}$$

Now one dimensional Lagrange polynomial defined as,

$$L_k(\eta) = \prod_{\substack{m=1 \\ m \neq k}}^{r} \frac{\eta - \eta_m}{\eta_k - \eta_m} \tag{27}$$

Obviously equation (equation 27) takes the value equal to zero at all points except at point *k (=1).* Here L_k (*k=1, 2, 3....r*), is Lagrange polynomial and ψ_k (*k=1, 2, 3*....) is the interpolation function or approximation function and η is the natural Coordinate whose value varies between -1 and 1. Now General Lagrange polynomial is written as follow,

$$L_k(\eta) = \frac{(\eta - \eta_1)(\eta - \eta_2).....(\eta - \eta_{k-1})(\eta - \eta_{k+1}).....(\eta - \eta_r)}{(\eta_k - \eta_1)(\eta_k - \eta_2).....(\eta_k - \eta_{k-1})(\eta_k - \eta_{k+1}).....(\eta_k - \eta_r)} \tag{28}$$

Now for three nodded element *(r = 3)*, shape function or interpolating function can be written as follow,

$$\psi_1 = \frac{-\eta(1-\eta)}{2}, \quad \psi_2 = 1-\eta^2, \quad \psi_3 = \frac{\eta(1+\eta)}{2}$$

Now putting the above expression of displacement variables into the governing equations, obtains the following equation of motion of the spinning shaft system as,

$$[M]\{\ddot{q}\} + ([C] + \Omega[G])\{\dot{q}\} + [K]\{q\} = \{F\} \tag{29}$$

Where, $[M]$ = Mass matrix, $[G]$ = Gyroscopic matrix, $[C]$ = Total damping matrix, $[K]$ = Structural Stiffness matrix, $\{q\}$ = Nodal Displacement vector, $\{F\}$ = External force vector. All the elemental matrices and vectors are given in appendix.

4.9 Contribution of Internal Damping

Based on Zorzi and Nelson [58], Qin and Mao [62] the derivation of rotor dynamic Lagrangian equation of motion including the contribution of both internal viscous and hysteretic damping of shaft disk element can be extended as,

$$[M]\{\ddot{q}\} + ([C] + \Omega[G] + \eta_V[K])\{\dot{q}\} + \left[\left(\frac{1+\eta_H}{\sqrt{1+\eta_H^2}}\right)[K] + \left(\eta_V\Omega + \frac{\eta_H}{\sqrt{1+\eta_H^2}}\right)[K_{Cir}]\right]\{q\} = \{F\} \tag{30}$$

Where K_{Cir} is the skew-symmetric circulation matrix. After assembly of the all elemental matrices, the equation of motion of the FG shaft can be obtained.

CHAPTER 5

RESULTS AND DISCUSSIONS

Based on the above formulation a complete MATLAB program has been developed and validated. Different types of analysis have been carried out and presented based on following problem specification.

5.1 Problem Specifications and Summarized of Various Analyses

Three disks rigidly mounted on shaft supported by two identical bearings has been modeled and analyzed using beam elements. All dimensions of this system are given in the Table 5.1. The shaft has been discretized by 13 elements (it is decided after convergence study). The stiffness and damping coefficients of each bearing are taken as $K_{yy} = 7\times10^7$ N/m, $K_{zz} = 5\times10^7$ N/m, $C_{yy} = 700$Ns/m, and $C_{zz} = 500$Ns/m at both ends. All the necessary data used in the present different analyses are given in Table 5.2 and Table 5.3.

The recent developed code has been validated with the results available in literatures. Various type of analysis for FG shaft have been studied and presented in the following sections. Firstly, it is shown that how temperature is distributed in radial direction of the FG shaft for different temperatures and power law gradient indexes. Secondly, the variation of mechanical properties (such as Young modulus, Poisson ratio, Thermal conductivity, coefficient of thermal expansion and mass density etc.) is presented for different radial position, different temperatures and power law gradient indexes. Thirdly, comparative study has been presented and discussed for FG shaft over steel shaft. Fourthly, the effects of power law gradient indexes have been analyzed for various responses of FG shaft. Fifthly, the effects of both power law gradient indexes and temperatures variations have been analyzed discussed for various responses of FG shaft. Finally, effect of both internal viscous and hysteretic damping have been carried out on the Campbell diagram.

Table 5.1 Mechanical properties and geometric dimension of steel rotor-shaft system [69]

Parameter	Shaft	Disk 1	Disk 2	Disk 3
Rotor shaft length (m)	1.3			
Rotor shaft diameter (mm)	100			
Young's Modulus (Gpa)	200			
Coefficient of viscous damping(s)	0.0002			
Coefficient of hysteretic damping	0.0002			
Eccentricity (m)			0.0002	
Density (Kg/m^3)	7800	7800	7800	7800
Outer diameter (m)		0.24	0.40	0.40
Thickness (mm)		5.0	5.0	6.0
Position from left end of rotor (m)		0.2	0.5	1.0

Table 5.2 Material properties of FGM compositions [79]

Properties	Stainless Steel (SUS304)	Aluminum oxide (Al_2O_3)
Young's Modulus *(GPa)*	210	390
Density *(Kg/m^3)*	7800	3960
Poisson Ratio	0.3	0.26

Table 5.3 Materials and temperature coefficients value for mechanical properties [34].

Property	Material	P_0	P_{-1}	P_1	P_2	P_3
E (Pa)	SUS304	201.0354e9	0	3.079296e-4	-6.533971e-7	0
	Al_2O_3	349.5486e9	0	-3.853206e-4	4.026993e-7	-1.6734e-10
K	SUS304	15.37895	0	-0.001264	0.20923e-5	-0.0722e-8
(W/m K)	Al_2O_3	-14.087	-1123.6	0.00044	0	0
CTE	SUS304	12.33e-6	0	0.0008	0	0
(1/K)	Al_2O_3	6.827e-5	0	0.00018	0	0
Poisson	SUS304	0.32622351	0	-2.001822e-4	3.797358e-7	0
ratio	Al_2O_3	0.26	0	0	0	0

5.2 Code Validation

In order to verify the FE developed code the following dimensions and mechanical properties were considered for steel shaft in Das [69] (details of which are given in Table 5.1). In order to convergence study of the result, it has been observed that result from the present code has been achieved an excellent agreement with the already published results of Das [69] and thus validates the correctness of the developed code. It is shown in Fig. 5.1.

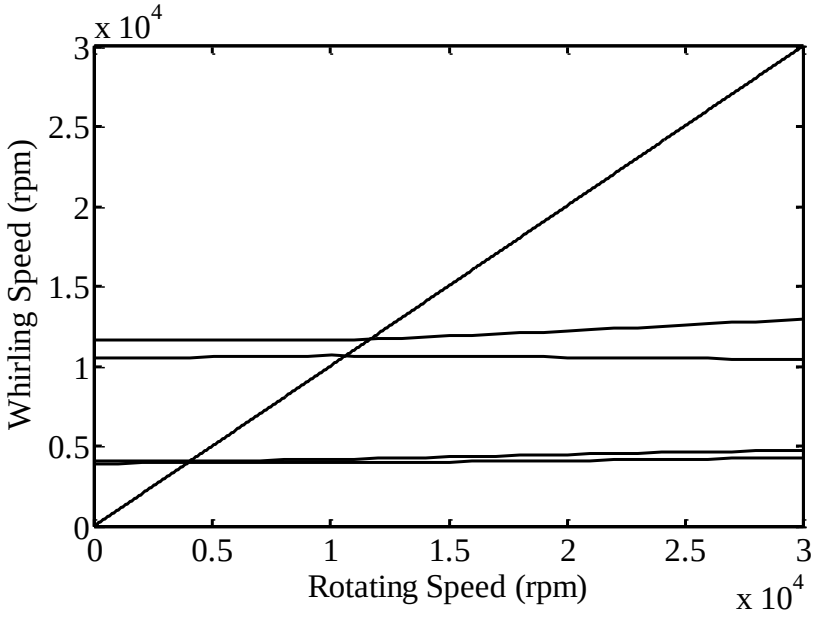

Fig. 5.1 Campbell diagram for first two pairs of modes

5.3 Temperature Distribution in a FG Shaft

The temperature distribution in FG layer is nonlinear which is clearly shown in Fig. 5. 2. This is due to that of thermal conductivity, coefficient of thermal expansion, modulus of elasticity and density which are the function of the radius of shaft only. For $k = 0$ and $k = \infty$, the temperature distribution is a straight line and does not depend upon the material properties of the shaft. For other values of k, the temperature distribution depends upon radial positions and material properties and also the law of gradation and it is presented in Table 5.4. From the Table 5.4, it is clear that from zero to one and one to ten values of k, temperature gradually decreases and increases respectively.

Table 5.4 Temperature variation of FG shaft for different radial position and power law gradient index (k)

r (m)	k	T_1 (K)	T_2 (K)	T_3 (K)	T_4 (K)	T_5 (K)	T_6 (K)
0.05	0.0	300	360	420	480	540	600
0.06	0.5	300	352.5686	409.6354	470.0942	533.6039	600
0.07	1.0	300	352.2281	407.8254	467.2561	531.0844	600
0.08	3.0	300	355.1254	410.7097	468.0016	529.4601	600
0.09	5.0	300	356.6653	413.3858	470.6490	530.5007	600
0.1	10	300	358.1465	416.2933	474.4676	533.2644	600

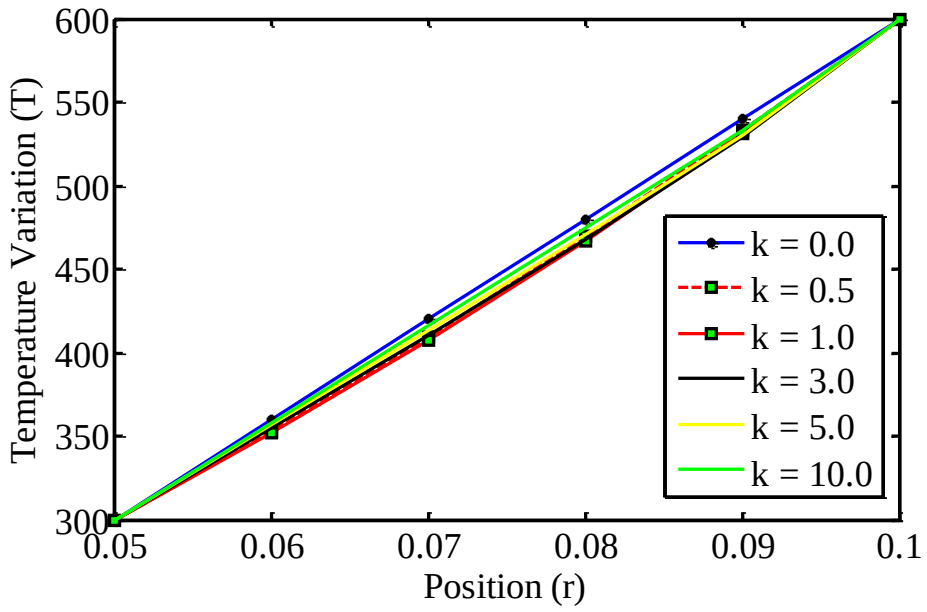

Fig. 5.2 Variation of temperature with radial position and power law gradient index

5.4 Variations of Mechanical Properties of FG Shaft with Positions and Temperatures

In the FG shaft model, shaft is composed of ceramic (aluminum oxide (Al_2O_3)) and metal (stainless steel (SUS304)) and its material property vary according to power law

gradation. Also aluminum oxide and stainless steel (SUS304) are considered at the top and the bottom surfaces of the shaft respectively. Now based on the above formulation it has been found that, for $k \to 0$ the material approaches to a homogeneous ceramic, and for $k \to \infty$ the material becomes entirely metal, for $0 < k < \infty$, the material will contain both metal and ceramic and for $k = 1$ ceramic and metal contribution is equal in the material. For a variation of mechanical properties, the required material properties and temperature coefficients of aluminum oxide and stainless steel are given in Table 5.1, Table 5.2 and Table 5.3 respectively. Now the Fig. 5.3, Fig. 5.4 and Fig. 5.5 show the mechanical properties of the FG shaft with various positions and power law gradient indexes (k).

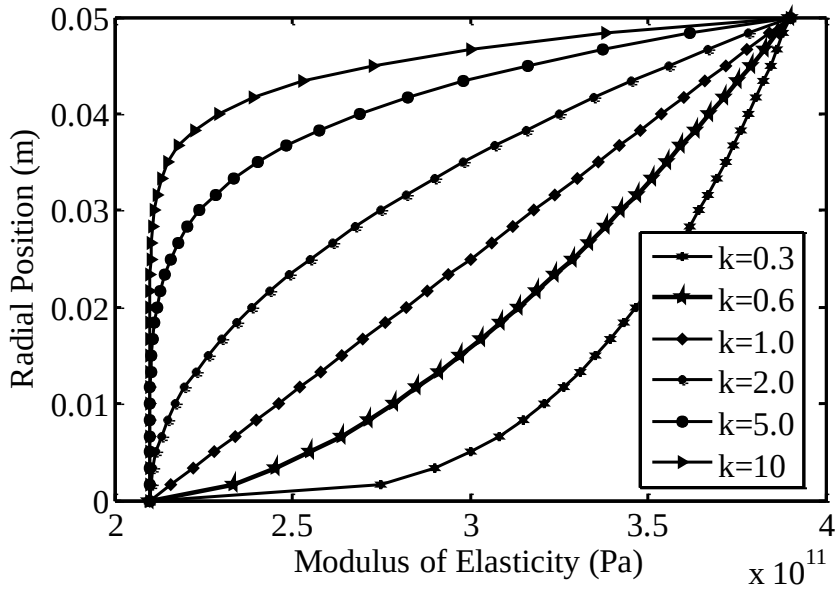

Fig. 5.3 Variation of Young modulus with power law gradient index of FG shaft

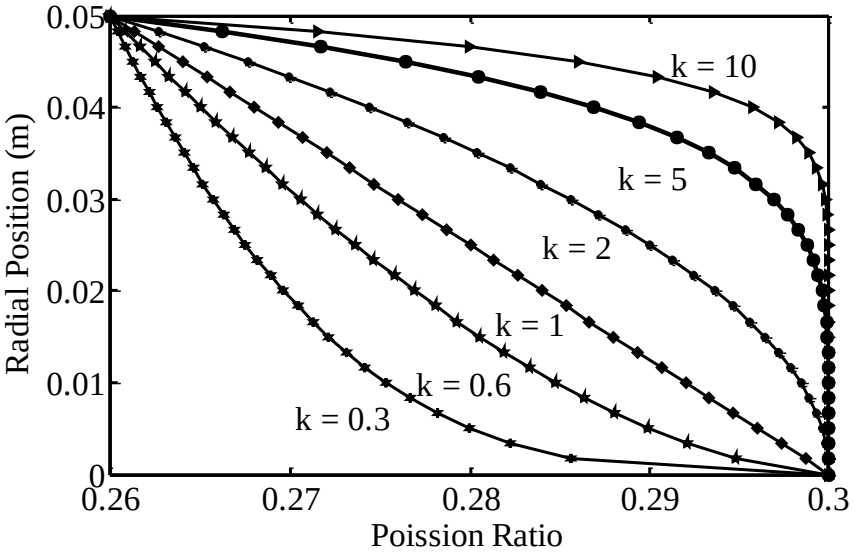

Fig. 5.4 Variation of Poisson ratio with power law gradient index of FG shaft

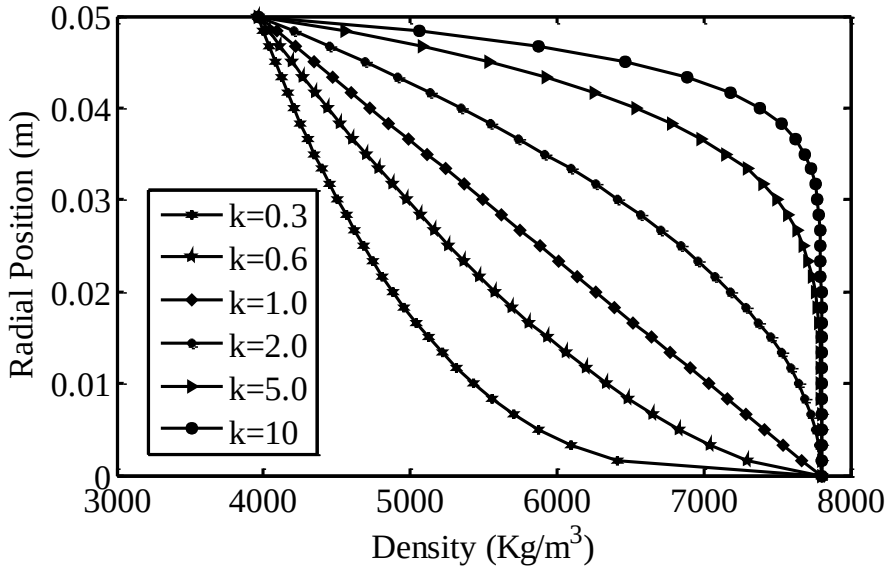

Fig. 5.5 Variation of density with power law gradient index of FG shaft

The mechanical properties of FG shaft with changing position, different temperatures and law of gradation index values are presented in the Table 5.5 and Table 5.6.

Table 5.5 Variation of Young's modulus with different radial positions, temperatures and power law gradient indexes of FG shaft

k	*T*(K)	*r* (m)	0	0.01	0.02	0.03	0.04	0.05
		E(10^{11}Pa)						
	300		3.2023	3.2023	3.2023	3.2023	3.2023	3.2023
0.0	420		3.1348	3.1348	3.1348	3.1348	3.1348	3.1348
	600		3.0678	3.0678	3.0678	3.0678	3.0678	3.0678
	300		2.0778	2.5807	2.7890	2.9489	3.0836	3.2023
0.5	420		2.0386	2.5288	2.7319	2.8877	3.0190	3.1348
	600		1.9089	2.4272	2.6418	2.8065	2.9454	3.0678
	300		2.0778	2.3027	2.5276	2.7525	2.9774	3.2023
1.0	420		2.0386	2.2579	2.4771	2.6963	2.9155	3.1348
	600		1.9089	2.1407	2.3724	2.6042	2.8360	3.0678
	300		2.0778	2.0782	2.0894	2.1653	2.4463	3.2023
5.0	420		2.0386	2.0390	2.0499	2.1239	2.3978	3.1348
	600		1.9089	1.9093	1.9208	1.9990	2.2886	3.0678
	300		2.0778	2.0778	2.0780	2.0846	2.1986	3.2023
10	420		2.0386	2.0386	2.0388	2.0453	2.1563	3.1348
	600		1.9089	1.9089	1.9090	1.9159	2.0333	3.0678

Table 5.6 Variation of thermal conductivity with different radial positions, temperatures and power law gradient indexes of FG shaft

k	*T*(K)	*r* (m)	0	0.01	0.02	0.03	0.04	0.05
		K(1/K)						
	300		36.814	36.814	36.814	36.814	36.814	36.814
0.0	420		20.9958	20.9958	20.9958	20.9958	20.9958	20.9958
	600		8.5743	8.5743	8.5743	8.5743	8.5743	8.5743
	300		12.1434	23.1765	27.7465	31.2532	34.2095	36.8140
0.5	420		12.0680	16.0606	17.7144	18.9835	20.0533	20.9958
	600		12.9010	10.9661	10.1646	9.5496	9.0311	8.5743
	300		12.1434	17.0775	22.0117	26.9458	31.8799	36.8140
1.0	420		12.0680	13.8536	15.6391	17.4247	19.2102	20.9958
	600		12.9010	12.0357	11.1703	10.3050	9.4396	8.5743
	300		12.1434	12.1513	12.3961	14.0618	20.2275	36.8140
5.0	420		12.0680	12.0709	12.1594	12.7622	14.9935	20.9958
	600		12.9010	12.8997	12.8567	12.5646	11.4832	8.5743
	300		12.1434	12.1434	12.1460	12.2926	14.7924	36.8140
10	420		12.0680	12.0680	12.0690	12.1220	13.0266	20.9958
	600		12.9010	12.9010	12.9006	12.8749	12.4365	8.5743

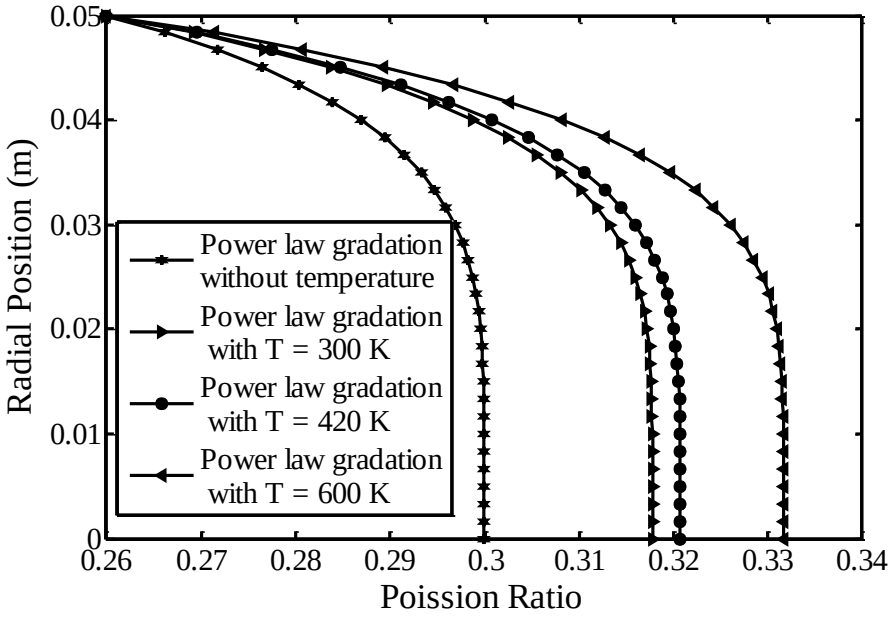

Fig. 5.6 Variation of Poisson ratio with different temperature and power law gradient index through radial direction of FG shaft

The Fig. 5.6 and Fig. 5.7 show the variation of Poisson's ratio and Young's Modulus with and without the temperature effect considering $k = 5.0$. From Fig. 5.6 It is clearly noticed that without the temperature, the values of Poisson's ratio less than that of considering temperature and it is increases with increasing temperature. From Fig. 5.7 It is clearly noticed that without the temperature, the values of Young's Modulus more than that of considering temperature and it is decreases with increasing temperature.

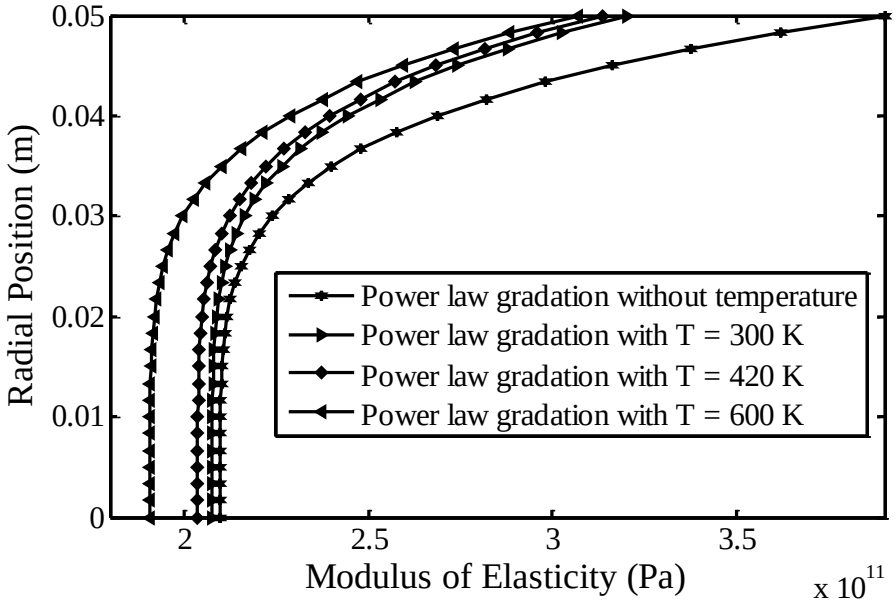

Fig. 5.7 Variation of Young modulus with different temperature and power law gradient index through radial direction of FG shaft

5.5 Comparative Studies of FG Shaft over Steel Shaft

For a comparative study of FG shaft over steel shaft all necessary data are given in Table 5.1, Table 5.2 and Table 5.3. Fig. 5.8 (a) and (b) show the comparison of Campbell diagram of FG shaft over steel shaft and it has been observed that the first critical speed occurs at 3891 rpm for steel shaft where as for FG shaft the first critical speed occurs at 4534 rpm. Fig. 5.9 (a) and (b) show the variation of maximum real part against speed of rotation for the FG and steel shafts respectively. It has been noticed that the maximum real part for steel shaft gives –17.45 rpm where as for the FG shaft it becomes –23.99 rpm. Fig. 5.10 (a) and (b) show the variation of damping ratio for first six modes of FG and steel shaft respectively. It has been observed that for the first forward mode of whirling damping ratio becomes negative at around 4756 rpm for steel shaft and beyond this speed it is unstable. And also for the first forward mode of whirling damping ratio becomes negative at around 10220 rpm for the FG shaft and beyond this speed it is unstable. So from the Fig. 5.8 (a) and (b), Fig. 5.9 (a) and (b) and Fig. 5.10 (a) and (b) it is evidently clear that the FG shaft is more stable than the steel shaft in same operating conditions.

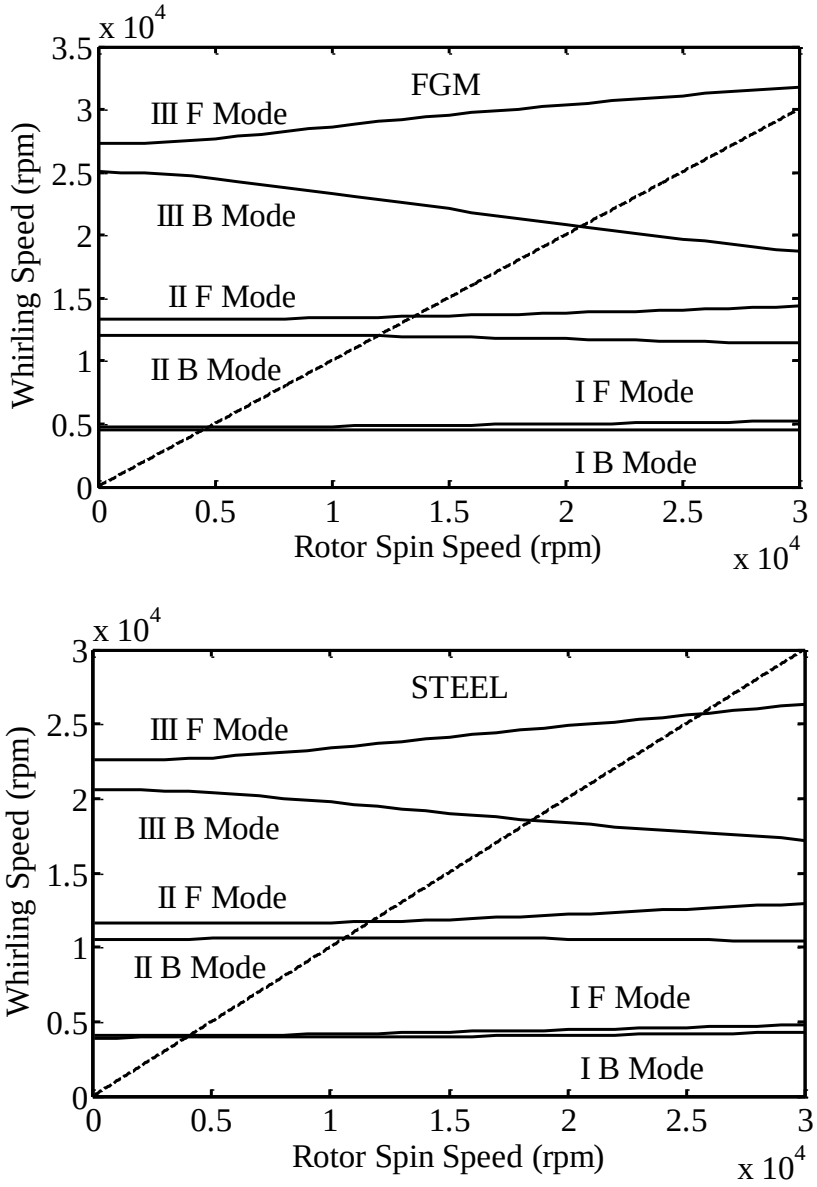

Fig. 5.8. Comparison of Campbell diagrams of rotating shafts: (a) FG and (b) Steel

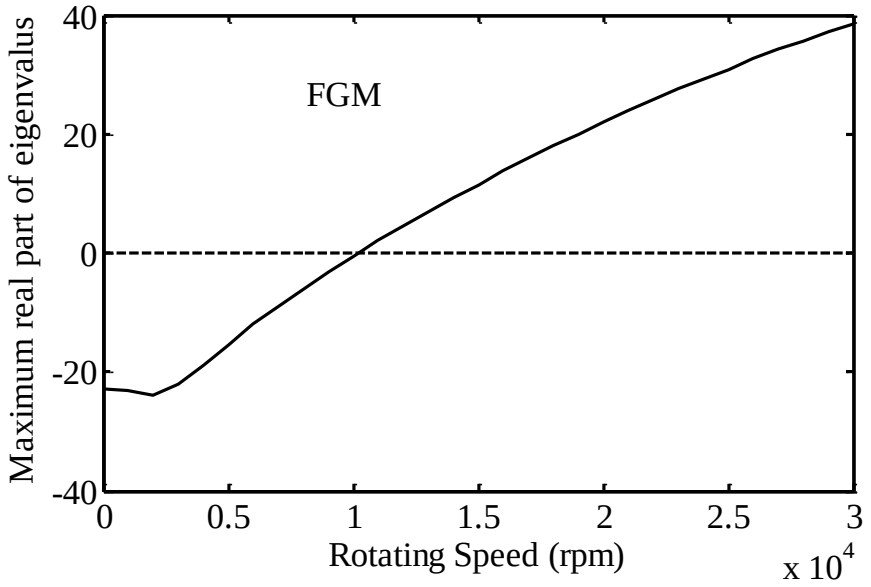

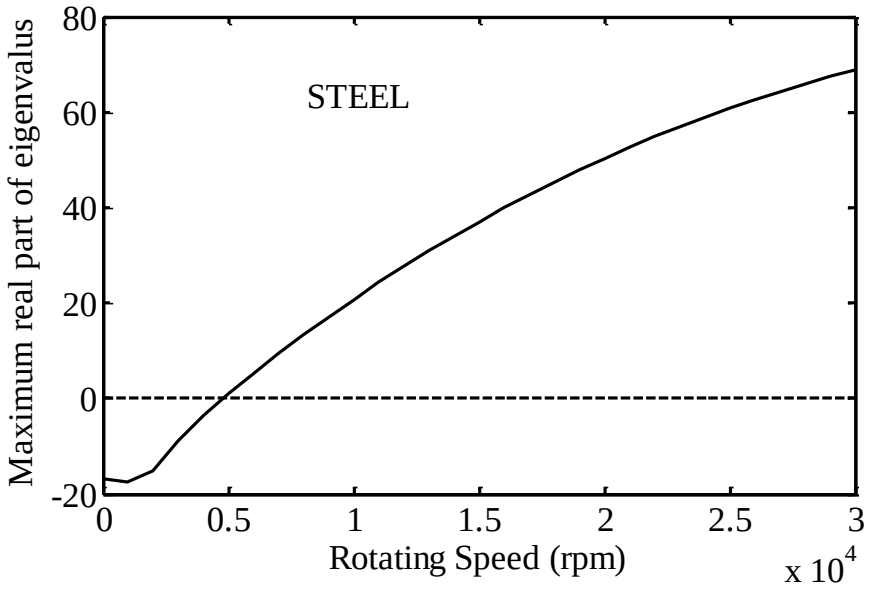

Fig. 5.9 Variation of maximum real part against speed of rotation: (a) FG and (b) Steel

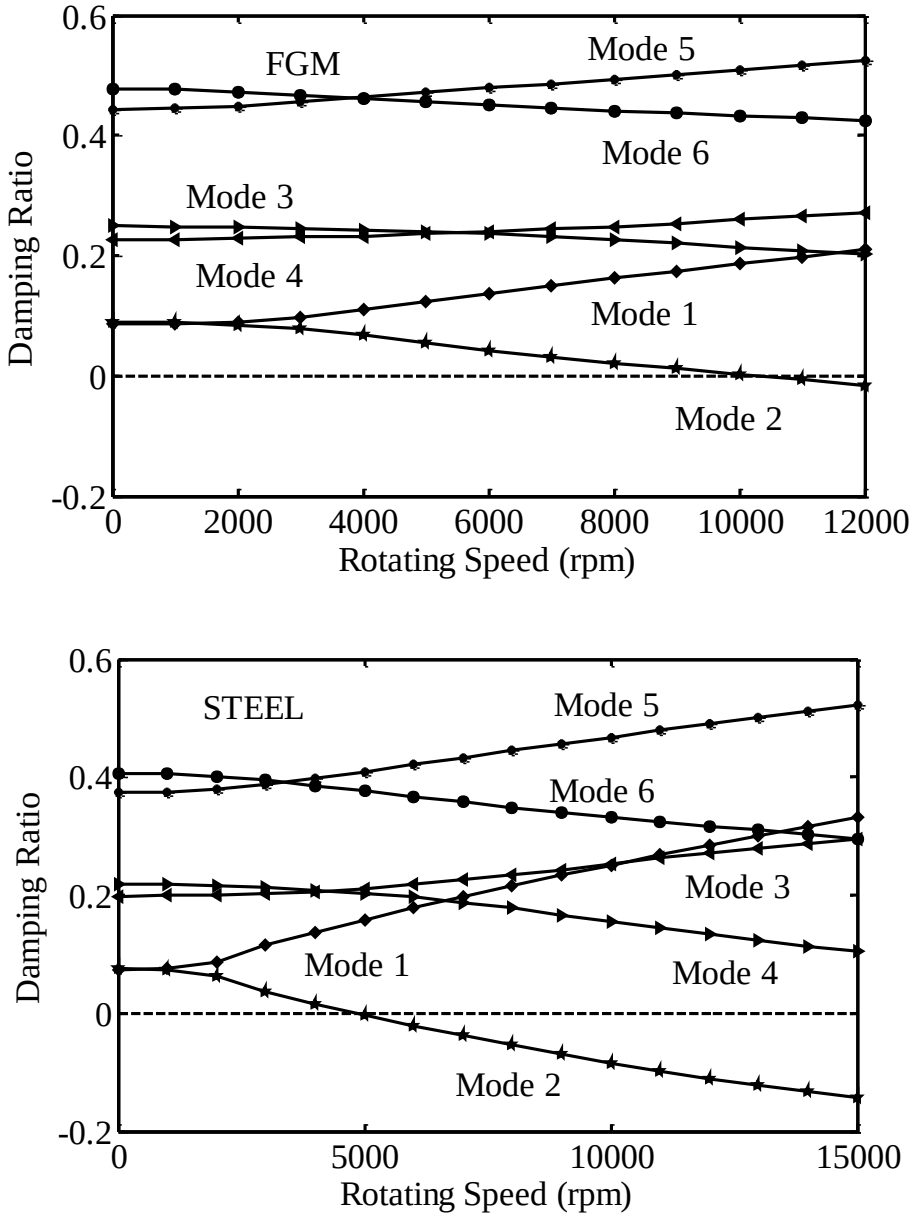

Fig. 5.10 Variation of damping ratio for the first six modes of rotating shafts:
(a) FG and (b) Steel

5.6 Comparative Studies of FG Shaft with and without Temperatures

For a comparative study of FG shaft over steel shaft, all necessary data are given in Table 5.1, Table 5.2 and Table 5.3. Fig. 5.11 (a) and (b) show the Campbell diagram of the FG shaft system considering with and without temperature effects and it has been observed that with temperature the first critical speed occurs at 4625.62 rpm where as for without temperature it becomes 4963.31rpm. Fig. 5.12 (a) and (b) also show the variation of maximum real part against speed of rotation of FG shaft considering with and without temperature effect respectively. It has been noticed that with temperature the maximum real part comes –25.187 rpm where as for without temperature it becomes –29.215 rpm.

Fig. 5.13 (a) and (b) show the variation of damping ratio for the first six modes of FG shaft considering with and without the temperature effect respectively. It has been observed that for the first forward mode of whirling damping ratio becomes negative at around 9853 rpm for with temperature where as at around 12000 rpm for without temperature and beyond this speed it is unstable. So from the Fig. 5.11 (a) and (b), Fig. 5.12 (a) and (b) and Fig. 5.13 (a) and (b) , it is evidently clear that without temperature the FG shaft is more stable.

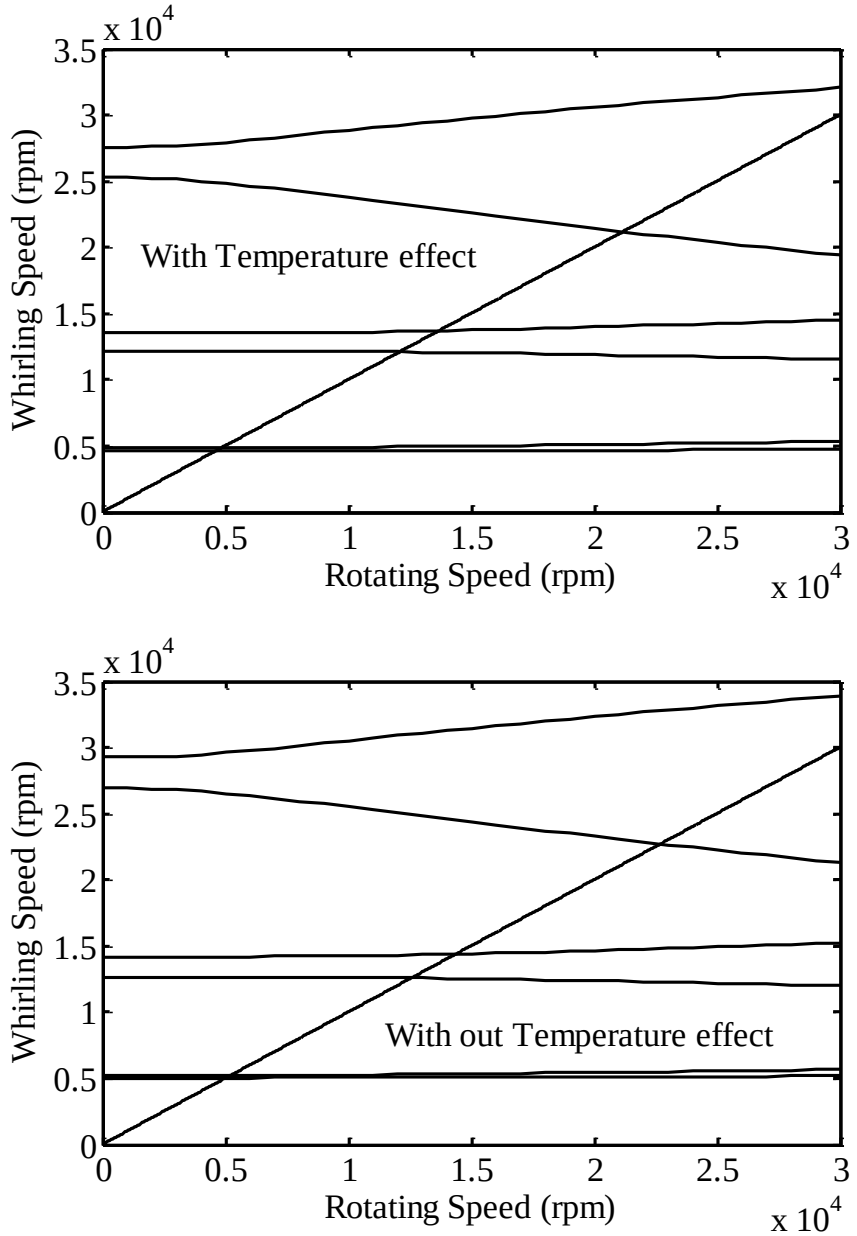

Fig. 5.11 Comparison of Campbell diagrams of rotating FG shafts: (a) with temperature and (b) without temperature

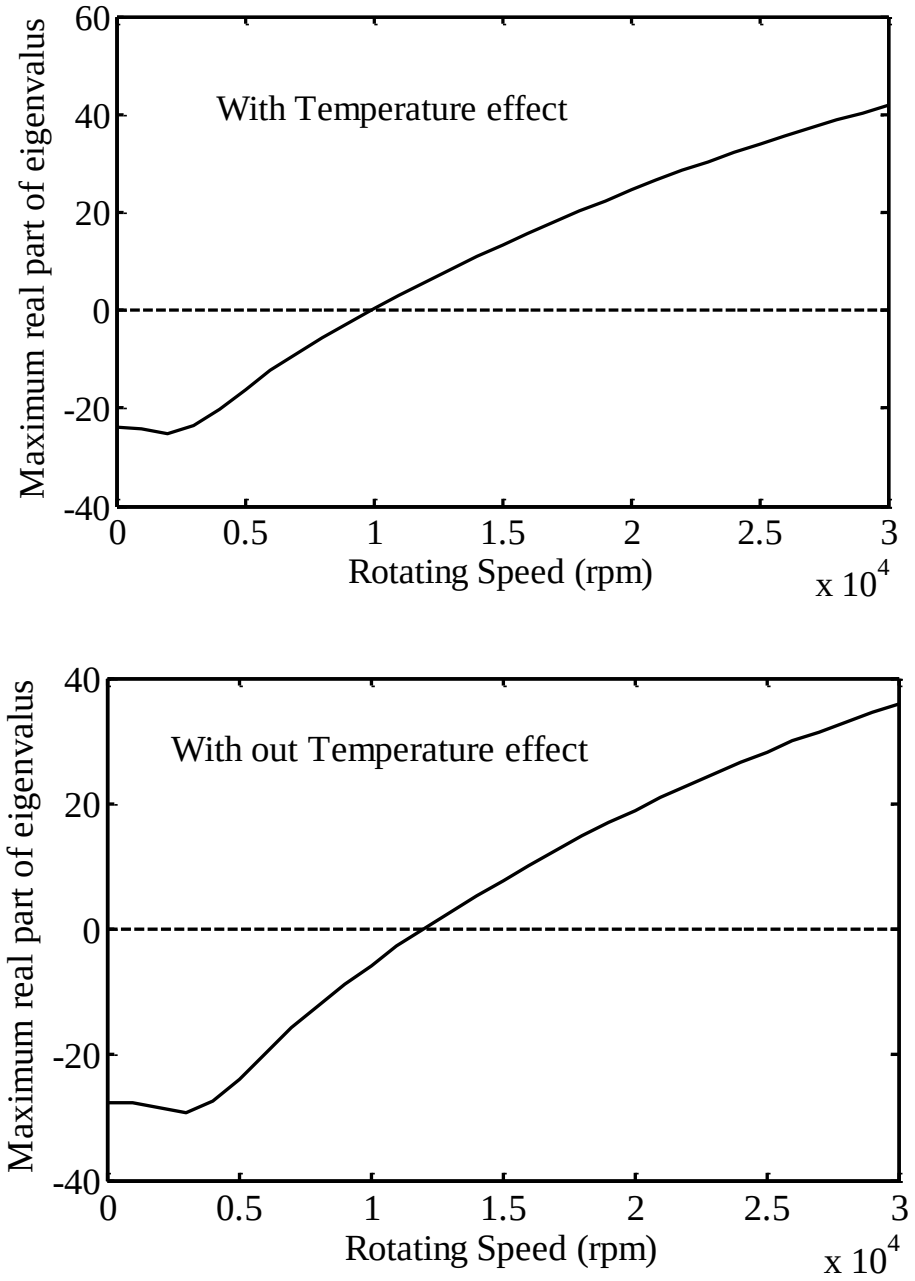

Fig. 5.12 Variation of maximum real part against speed of rotation of FG shaft: (a) with temperature and (b) without temperature

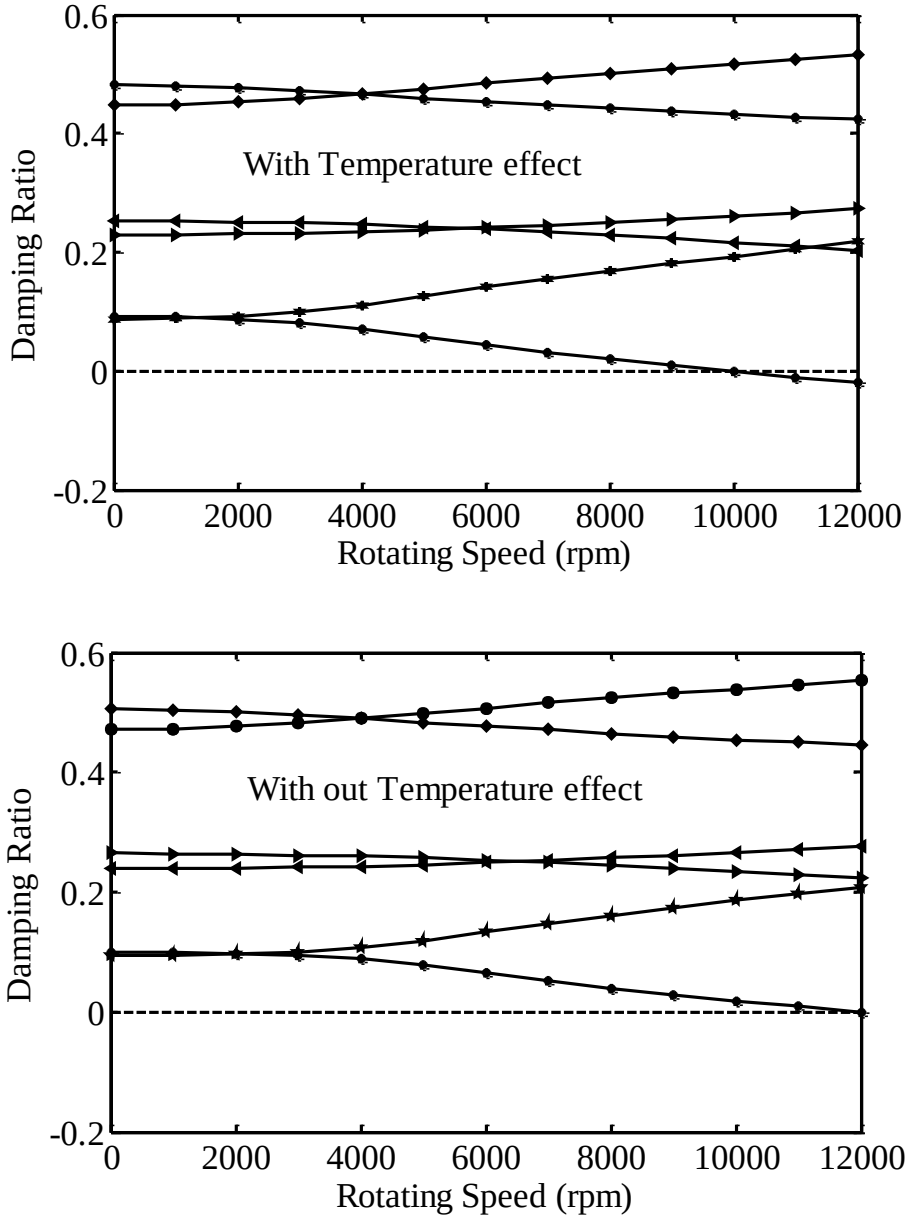

Fig. 5.13 Variation of damping ratio for the first six modes of rotating FG shaft: (a) with temperature and (b) without temperature

5.7 The Effect of Different Gradient Indexes on Various Responses of FG Shaft

In order to study the responses of FG shaft all others necessary data are given in Table 5.1, Table 5.2 and Table 5.3. From the Fig. 5.14 (a) and (b), it has been found that the first critical speed occurs at 4581.56 rpm for $k=10$ where as for $k=5$ the first critical speed occurs at 4687.68 rpm. Fig. 5.15 (a) and (b) show that the maximum real part is -25.67 rpm for $k=5$ and for $k=10$ it comes -24.67 rpm. From the Fig. 5.16 (a) and (b), it is clear that the first forward mode of whirling damping ratio becomes negative at around 11180 rpm for $k=5$ and for $k=10$, it comes 10580 rpm and beyond these speeds it is unstable.

The Table 5.7 indicates the significance of the power law gradient index in vibration and stability analysis of FG shaft. It is observed from this analysis, the less value of the power law gradient index gives more stable system than that the higher value of the power law gradient index.

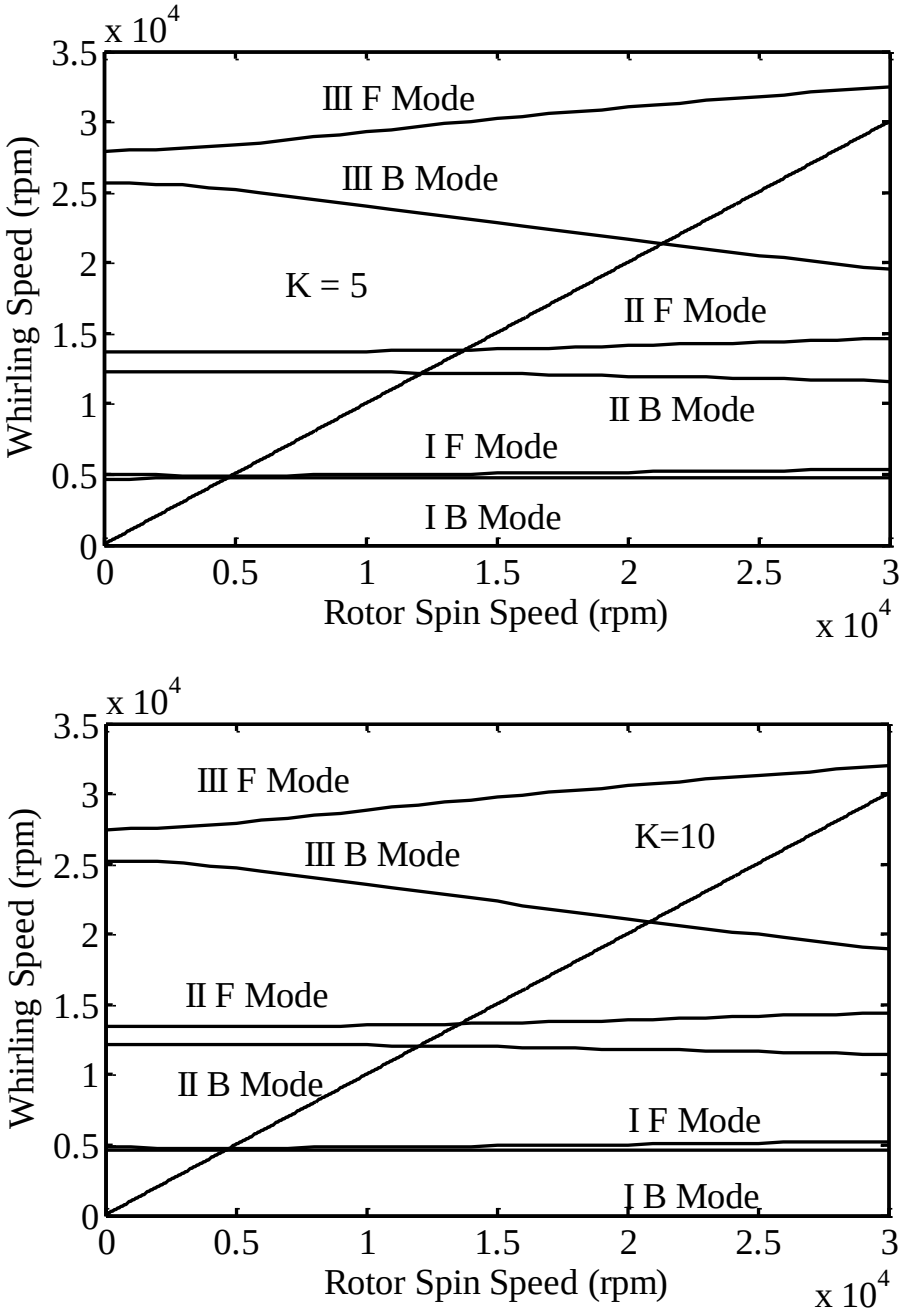

Fig. 5.14 The Campbell diagram of FG shaft: (a) $k = 5$ and (b) $k = 10$

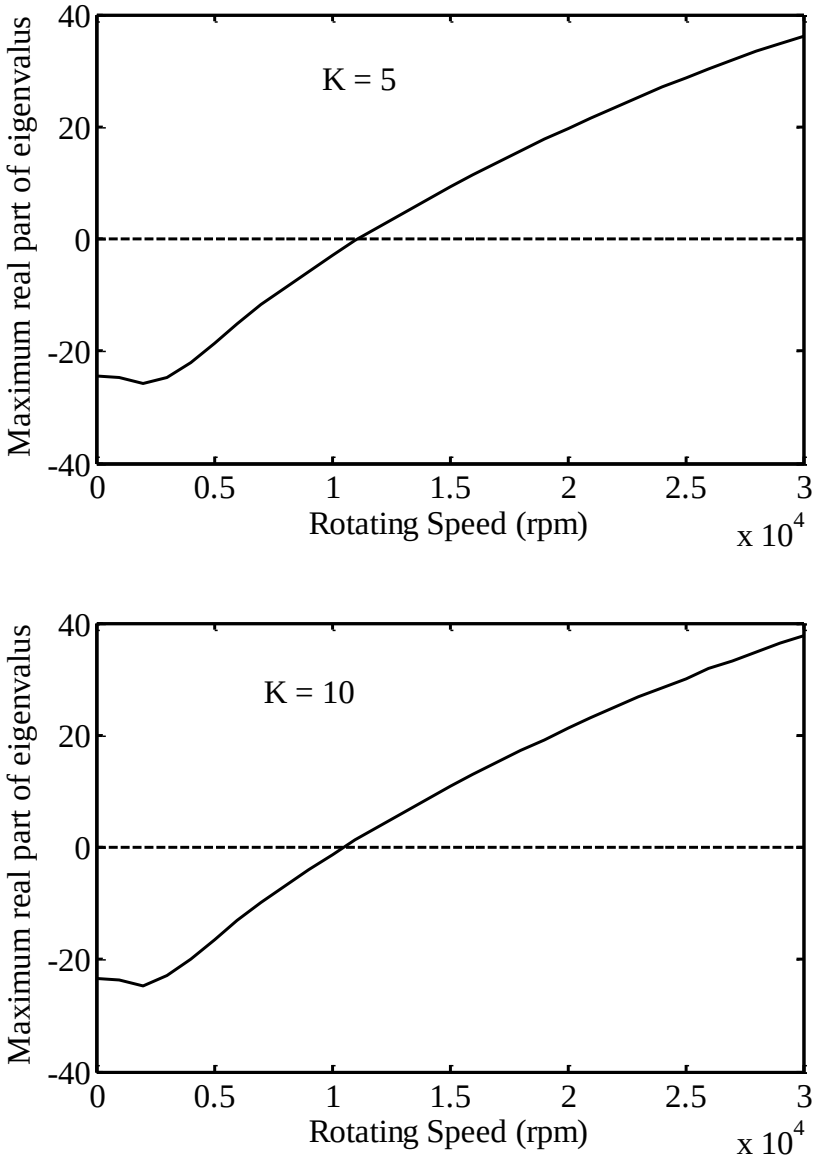

Fig. 5.15 The maximum real part against spin speed of FG shaft: (a) $k = 5$ and (b) $k = 10$

Table 5.7 First critical speed and maximum real part for different power law gradient indexes

k	First critical speed (rpm)	Max. Real part	*k*	First critical speed (rpm)	Max. Real part
0.0	5025.45	–30.216	5.0	4687.68	–25.672
0.5	4963.31	–29.215	7.0	4633.50	–25.176
1.0	4911.76	–28.382	10.0	4581.56	–24.674
3.0	4770.93	–26.465	15.0	4534.16	–23.990

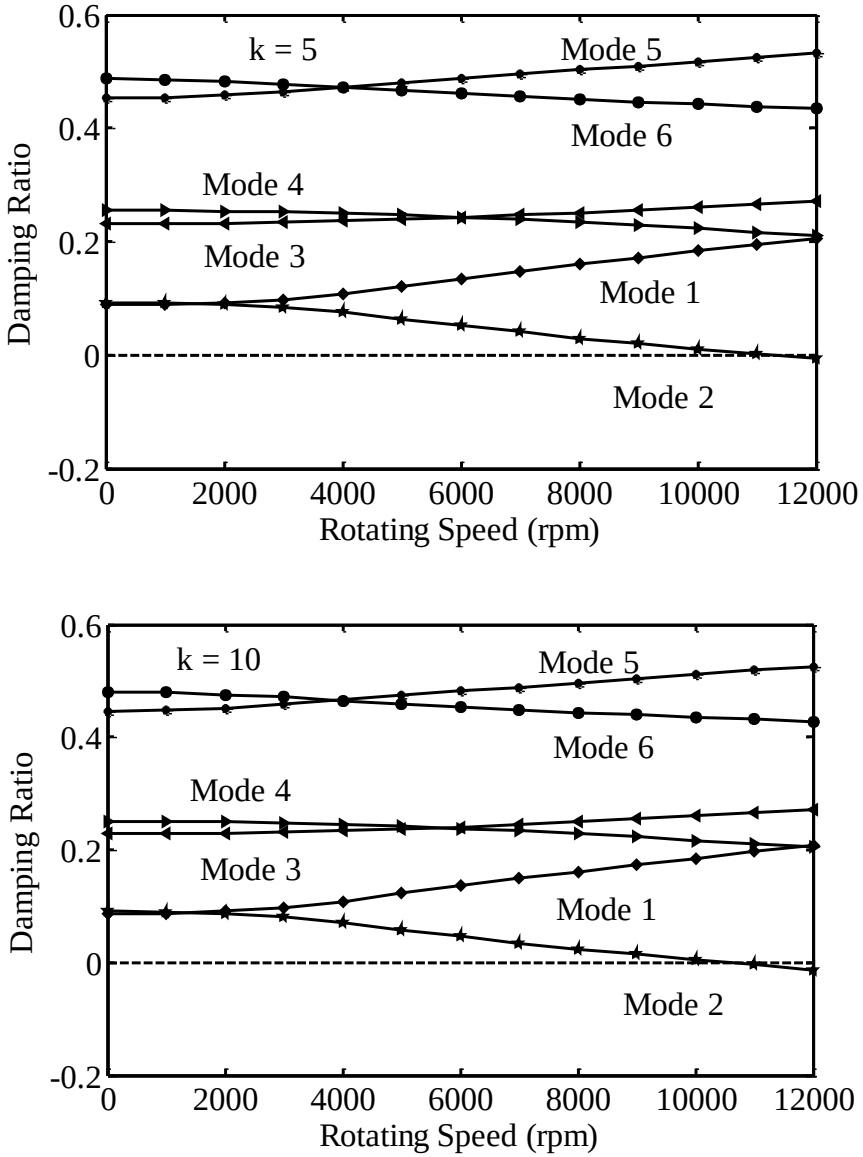

Fig. 5.16 The damping ratio of first six modes of FG shaft: (a) $k = 5$ and (b) $k = 10$

5.8 The Effects of Different Temperatures and Gradient Indexes on Various Responses of FG Shaft

In order to obtain the FG shaft responses the power law gradient index is considered $k = 0.5$ and all others necessary data are given in Table 5.1, Table 5.2 and Table 5.3. From the Fig. 5.17 (a) and (b) , it has been found that first critical speed occurs at 4625.62 rpm for $T = 300K$ where as for $T = 600K$ the first critical speed occurs at 4554.67 rpm. Fig. 5.18 (a) and (b) show that the maximum real part is -25.19 rpm for $T = 300K$ where as for $T = 600K$ it becomes -24.26 rpm. Now from Fig. 5.19 (a) and (b), it is clear that the first forward mode of whirling damping ratio becomes negative at around 9877 rpm where as for $T = 300K$ and for $T = 600K$ it becomes 9623 rpm and beyond these speeds it is unstable.

The Table 5.8 indicates the significance of both the values of temperature and the power law gradient index on the vibration and stability analysis. The temperature and power law gradient index have a significant role in the responses of FG shaft. It is also clear from this analysis that less value of temperature and the power law gradient index gives more stable system than that of higher values of temperature and power law gradient index.

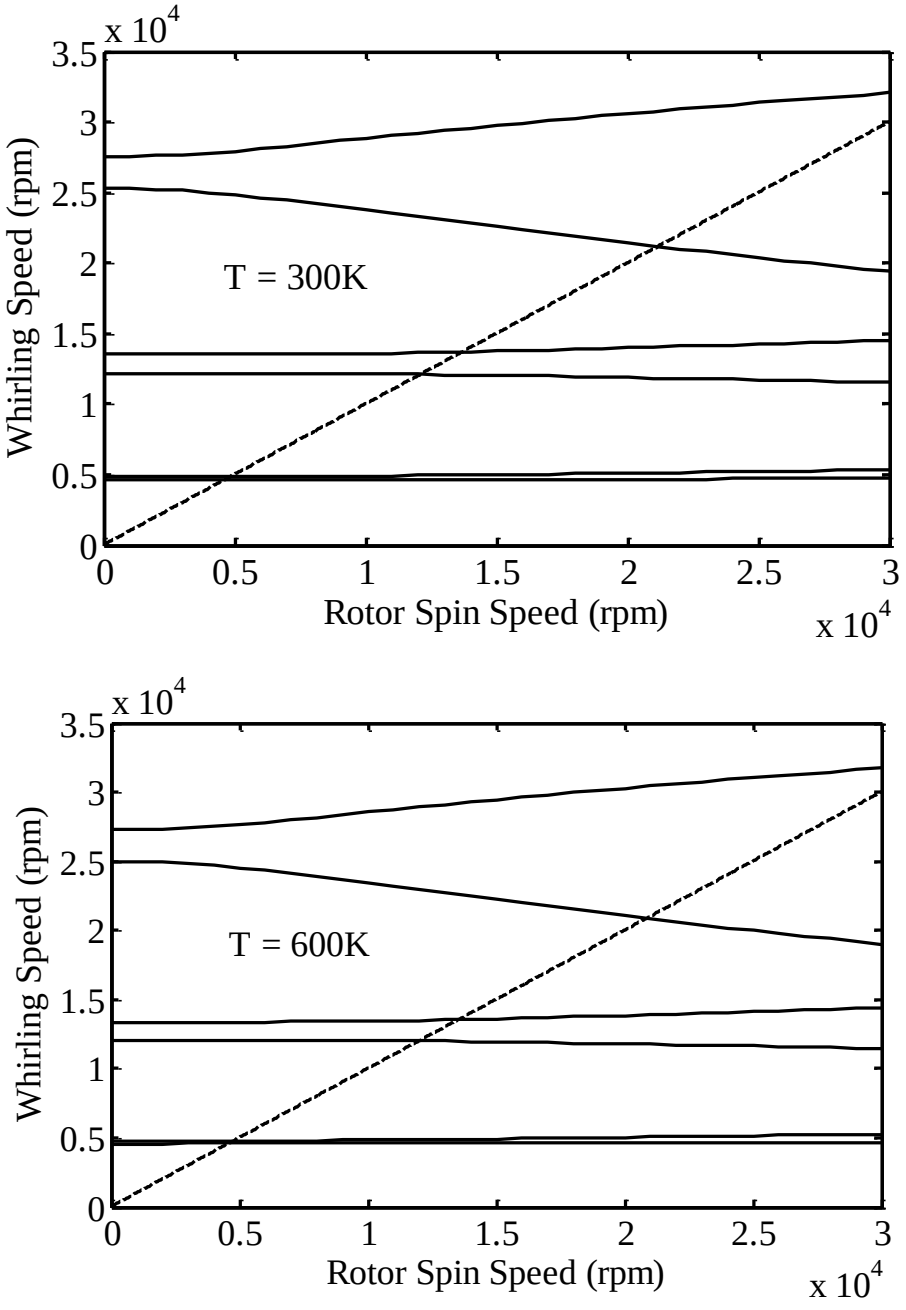

Fig. 5.17 The Campbell diagram of FG shaft: (a) $T = 300K$ and (b) $T = 600K$

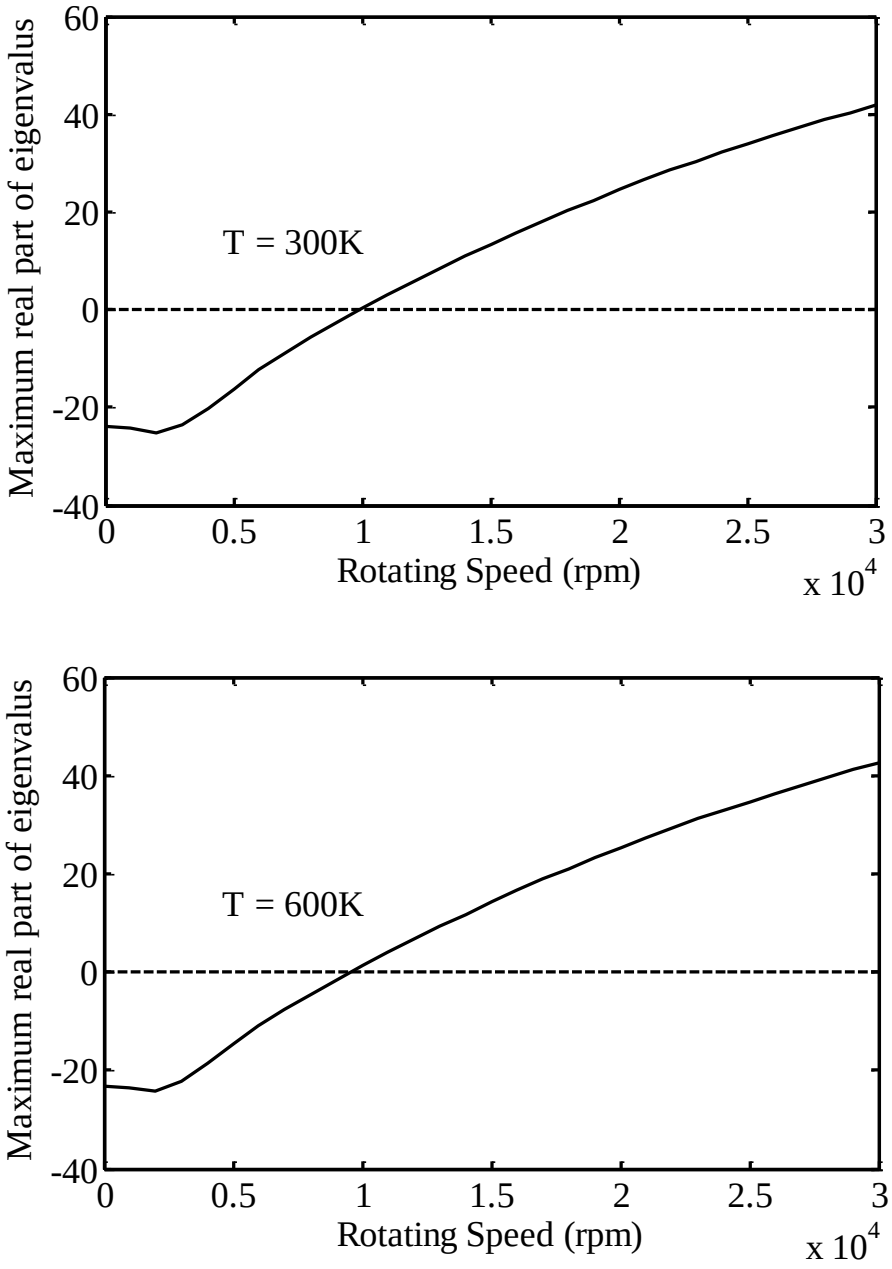

Fig. 5.18 Maximum real part against spin speed of FG shaft:
(a) $T = 300K$ and (b) $T = 600K$

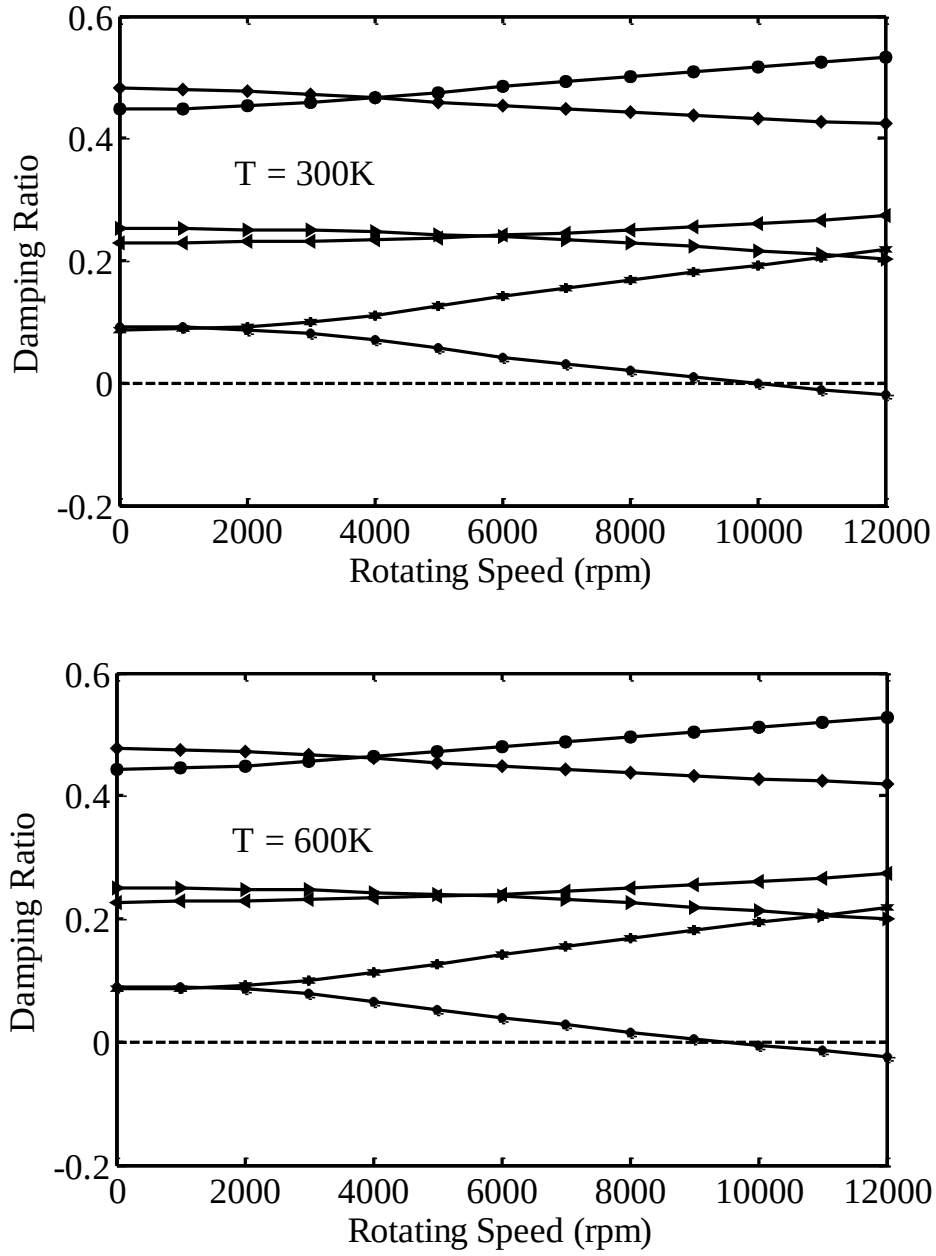

Fig. 5.19 Damping ratio for first six modes of FG shaft: (a) $T = 300K$ and (b) $T = 600K$

Table 5.8 First critical speed and maximum real part for different values of temperatures and power law gradient indexes (k)

k	$T(K)$	First critical speed (rpm)	Max. Real part	k	$T(K)$	First critical speed (rpm)	Max. Real part
	300	4733.41	–26.269		300	4286.47	–20.948
	360	4716.22	–26.113		360	4272.23	–20.752
0.0	420	4701.49	–25.981	3.0	420	4256.29	–20.563
	480	4688.93	–25.869		480	4238.41	–20.398
	540	4678.25	–25.774		540	4218.31	–20.213
	600	4669.09	–25.693		600	4195.69	–20.007
	300	4625.62	–25.187		300	4131.17	–19.406
	360	4609.06	–25.042		360	4118.06	–19.290
0.5	420	4593.98	–24.823	5.0	420	4101.88	–19.147
	480	4580.08	–24.621		480	4082.37	–18.976
	540	4567.09	–24.434		540	4059.25	–18.773
	600	4554.67	–24.256		600	4032.19	–18.538
	300	4536.28	–24.112		300	3918.55	–17.534
	360	4520.29	–23.881		360	3907.02	–17.439
1.0	420	4504.95	–23.661	10.0	420	3890.65	–17.303
	480	4489.97	–23.449		480	3869.21	–17.127
	540	4475.07	–23.239		540	3842.39	–16.907
	600	4459.94	–23.029		600	3809.84	–16.644

5.9 Time Responses for FG Shaft System due to Unbalance Masses

The Fig. 5.20 (a) and (b) show the displacement histories (stable and unstable responses) due to unbalance masses in transverse directions for the index of $k = 0.5$ and $T = 300K$. Here, the time responses in the transverse directions of this shaft have also been obtained considering the unbalance mass of the disk 2 and the responses of this system have been calculated with a time step of τ/10 s (where τ is the time period corresponding to the first natural frequency of the system). Finally from the Fig. 5.20 (a) and (b) , it is clear that for stable response the maximum amplitude is 5.676×10^{-5} m and for unstable response the maximum amplitude is 1.897×10^{-4} m and also from Table 5.9, it is found that for both the less values of the power law gradient index as well as the temperature variations, the maximum amplitude is less, thus it promotes more stable system than that of higher values of power law gradient and temperature variations.

Table 5.9 Maximum amplitudes for different temperatures and power law gradient index (k)

		Stable response		Unstable response	
		Max. Amplitude (10^{-5} m)		Max. Amplitude (10^{-4} m)	
k	T(K)	V- direction	W- direction	V- direction	W- direction
0.0	300	8.762	6.935	2.406	2.004
	420	8.330	6.593	2.896	2.359
	600	7.980	6.351	3.801	3.205
0.5	300	7.164	5.676	2.207	1.897
	420	6.883	5.556	2.651	2.418
	600	6.371	5.291	3.297	2.806
1.0	300	6.188	5.005	2.530	2.229
	420	5.959	4.868	3.139	2.716
	600	5.391	4.729	3.832	3.168
3.0	300	4.230	3.844	5.327	5.023
	420	4.084	3.795	6.520	5.975
	600	3.950	3.629	7.137	6.727
5.0	300	3.579	3.268	10.06	9.428
	420	3.539	3.092	11.75	9.800
	600	3.376	3.023	13.68	12.67
10.0	300	2.806	2.729	23.55	21.92
	420	2.678	2.413	26.97	24.91
	600	2.602	2.202	31.43	29.41

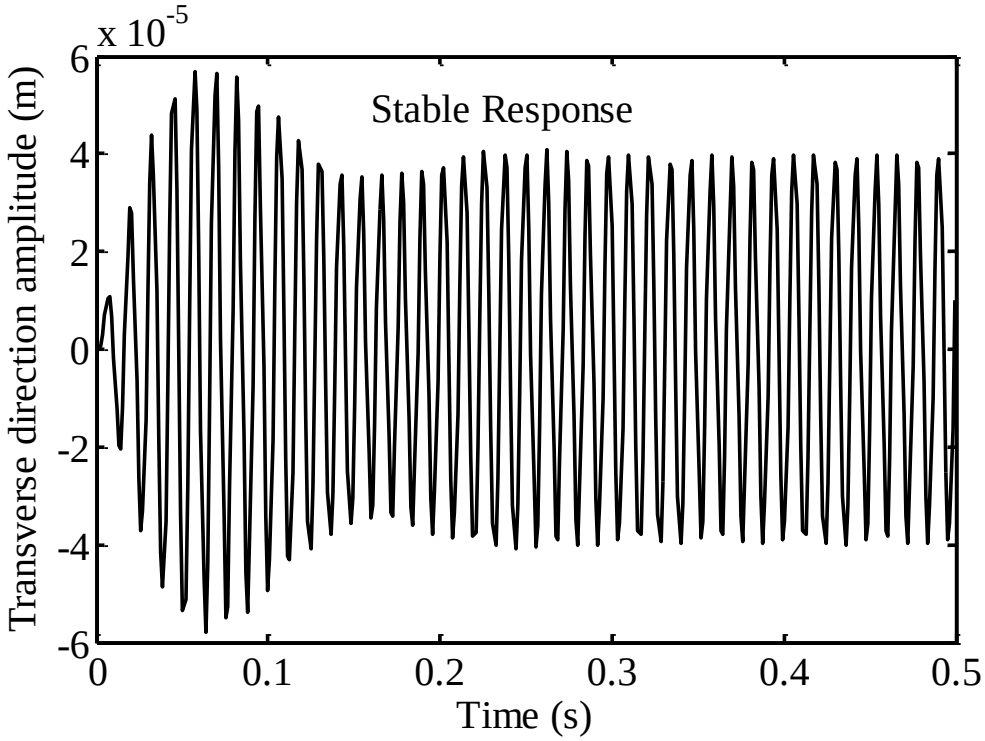

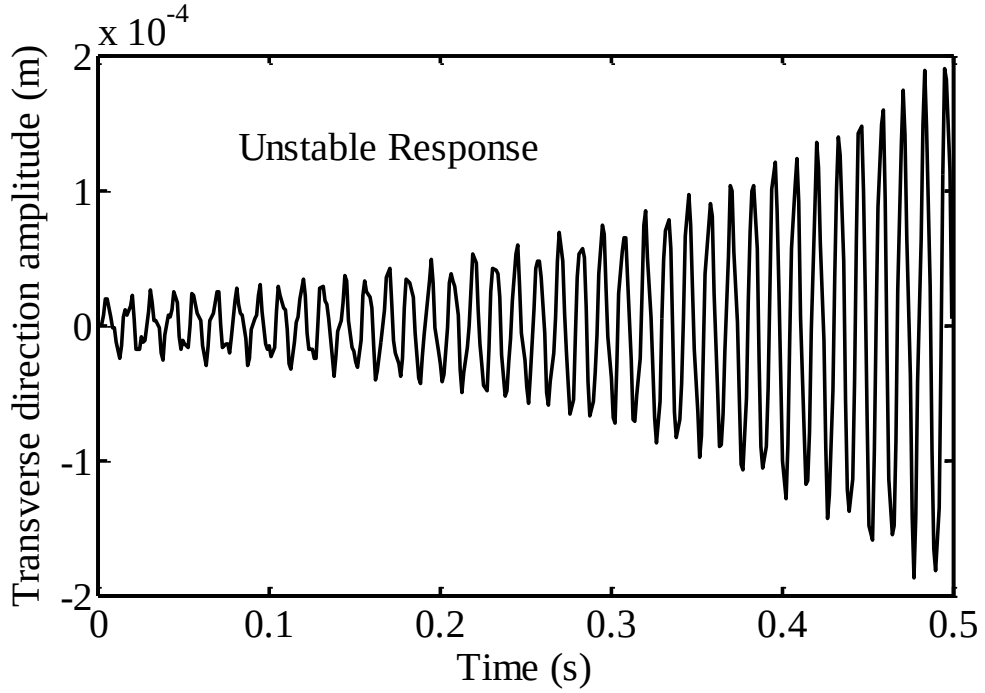

Fig. 5.20. Displacement histories due to unbalance masses along the transverse direction of FG shaft: (a) stable response and (b) unstable response

CHAPTER 6

Conclusions and Scope of Further Works

This chapter presents few important observations based on the vibration and stability analysis of the FG spinning shaft system using developed MATLAB code. Scope of further work in this direction has also been presented at the end of this chapter.

6.1 Conclusions

The present work enables to arrive at the following important conclusions:

- A three nodded beam finite element has been implemented for modeling and vibration analysis of the FG shaft system by incorporating both the internal viscous and hysteretic damping in the thermal environment.

- The temperature distribution is nonlinear along the radial direction of the cross-section of FG shaft.

- The material property distribution of the FG shaft has been performed very smoothly along the radial direction by accounting different temperatures and power law gradient indexes.

- From the comparison of various responses between steel and FG shaft, it has been found that FG shaft is more stable than the steel shaft.

- From the comparison of various responses of the FG shaft without and with temperatures consideration, it has been noticed that the FG shaft is more stable in case of without temperature consideration than that of with temperature consideration.

- The power law gradient index plays an important role in the responses (viz. Campbell diagram, damping ratio, critical speed, stability limit speed and time responses) of the FG shaft system.

- It is observed that the less value of temperature and the power law gradient index promotes more stable system than that of higher values of temperature and power law gradient index
- Finally, it can be concluded that the present work can be used for modeling and vibration analysis of the FG shaft system considering with or without temperature dependent material properties according to power law gradation by incorporating both internal viscous and hysteretic damping.

6.2 Scope of Future Works

- Study of vibration and stability analysis for FG rotor shaft system under electro-thermo-mechanical environment.
- Study of vibration and stability analysis by using a fluid film journal bearing for this present model
- Active vibration control of FG rotor shaft system
- Nonlinear modeling of FG shaft and
- Multiobjective optimization of FG shaft system

Appendix

The terms A_{11}, A_{55}, A_{66}, B_{11} of the equation (19) and I_m, I_d, I_p of the equation (20) given as follows:

$$A_{55}=\frac{\pi}{2}\sum_{i=1}^{k}\overline{C}_{55r}\left(r^2{}_{i+1}-r^2{}_{i}\right),\quad A_{66}=\frac{\pi}{2}\sum_{i=1}^{k}\overline{C}_{66r}\left(r^2{}_{i+1}-r^2{}_{i}\right)$$

$$A_{16}=\frac{2\pi}{3}\sum_{i=1}^{k}\overline{C}_{16r}\left(r^3{}_{i+1}-r^3{}_{i}\right),\quad B_{11}=\frac{\pi}{4}\sum_{i=1}^{k}\overline{C}_{11r}\left(r^4{}_{i+1}-r^4{}_{i}\right)$$

$$I_m=\pi\sum_{i=1}^{k}\rho_i\left(r^2{}_{i+1}-r^2{}_{i}\right),\quad I_d=\frac{\pi}{4}\sum_{i=1}^{k}\rho_i\left(r^4{}_{i+1}-r^4{}_{i}\right),\quad I_p=\frac{\pi}{2}\sum_{i=1}^{k}\rho_i\left(r^4{}_{i+1}-r^4{}_{i}\right)$$

$$\overline{C}_{11r}=\frac{E}{1-\nu^2},\quad \overline{C}_{16r}=\frac{\nu E}{1-\nu^2},\quad \overline{C}_{55r}=\overline{C}_{66r}=\frac{E}{2(1+\nu)}$$

Where k is the number of layer in the laminate and r_{i+1} and r_i are represents outer and inner radii of the i^{th} layer of the laminate respectively. ρ_i is the density of the composite shaft of i^{th} layer. Now various matrices of the equation (34) can be written as follows:

Nodal displacements vector:

$$\{q_e\}^T=\left\{\{v_e\}^T_{1\times3}\{w_e\}^T_{1\times3}\{\beta_{xe}\}^T_{1\times3}\{\beta_{ye}\}^T_{1\times3}\right\}_{1\times12}$$

Mass Matrices:

$$[M_e]=\begin{bmatrix}[M_v]_{3\times3} & [0]_{3\times3} & [0]_{3\times3} & [0]_{3\times3}\\ [0]_{3\times3} & [M_w]_{3\times3} & [0]_{3\times3} & [0]_{3\times3}\\ [0]_{3\times3} & [0]_{3\times3} & [M_{\beta_x}]_{3\times3} & [0]_{3\times3}\\ [0]_{3\times3} & [0]_{3\times3} & [0]_{3\times3} & [M_{\beta_y}]_{3\times3}\end{bmatrix}_{12\times12}$$

$$[M_v]=I_m\int_{x_i}^{x_f}[\Psi]^T[\Psi]dx+I_m^D\int_{x_i}^{x_f}\sum_{i=1}^{N_D}[\Psi]^T[\Psi]\Delta(x-x_{Di})dx$$

$$[M_w]=I_m\int_{x_i}^{x_f}[\Psi]^T[\Psi]dx+I_m^D\int_{x_i}^{x_f}\sum_{i=1}^{N_D}[\Psi]^T[\Psi]\Delta(x-x_{Di})dx$$

$$\left[M_{\beta_x}\right] = I_d \int_{x_i}^{x_f} [\Psi]^T [\Psi] dx + I_d^D \int_{x_i}^{x_f} \sum_{i=1}^{N_D} [\Psi]^T [\Psi] \Delta(x - x_{Di}) dx$$

$$\left[M_{\beta_y}\right] = I_d \int_{x_i}^{x_f} [\Psi]^T [\Psi] dx + I_d^D \int_{x_i}^{x_f} \sum_{i=1}^{N_D} [\Psi]^T [\Psi] \Delta(x - x_{Di}) dx$$

Stiffness Matrix:

$$[K_e] = \begin{bmatrix} [K_{vv}]_{3\times3} & [0]_{3\times3} & \left[K_{v\beta_x}\right]_{3\times3} & \left[K_{v\beta_y}\right]_{3\times3} \\ [0]_{3\times3} & [K_{ww}]_{3\times3} & \left[K_{w\beta_x}\right]_{3\times3} & \left[K_{w\beta_y}\right]_{3\times3} \\ \left[K_{v\beta_x}\right]_{3\times3}^T & \left[K_{w\beta_x}\right]_{3\times3}^T & \left[K_{\beta_x\beta_x}\right]_{3\times3} & \left[K_{\beta_x\beta_y}\right]_{3\times3} \\ \left[K_{v\beta_y}\right]_{3\times3}^T & \left[K_{w\beta_y}\right]_{3\times3}^T & \left[K_{\beta_x\beta_y}\right]_{3\times3}^T & \left[K_{\beta_y\beta_y}\right]_{3\times3} \end{bmatrix}_{12\times12}$$

$$[K_{vv}] = \int_{x_i}^{x_f} \left\{ K_s (A_{55} + A_{66}) \left[\Psi'\right]^T \left[\Psi'\right] + \sum_{i=1}^{N_B} K_{yy}^{Bi} [\Psi]^T [\Psi] \Delta(x - x_{Bi}) \right\} dx$$

$$[K_{ww}] = \int_{x_i}^{x_f} \left\{ K_s (A_{55} + A_{66}) \left[\Psi'\right]^T \left[\Psi'\right] + \sum_{i=1}^{N_B} K_{zz}^{Bi} [\Psi]^T [\Psi] \Delta(x - x_{Bi}) \right\} dx$$

$$\left[K_{\beta_x\beta_x}\right] = \int_{x_i}^{x_f} \left\{ K_s (A_{55} + A_{66}) [\Psi]^T [\Psi] + D_{11} \left[\Psi'\right]^T \left[\Psi'\right] \right\} dx$$

$$\left[K_{\beta_y\beta_y}\right] = \int_{x_i}^{x_f} \left\{ K_s (A_{55} + A_{66}) [\Psi]^T [\Psi] + D_{11} \left[\Psi'\right]^T \left[\Psi'\right] \right\} dx$$

$$\left[K_{v\beta_x}\right] = \left(-\frac{1}{2} K_s B_{16}\right) \int_{x_i}^{x_f} \left[\Psi'\right]^T \left[\Psi'\right] dx \quad \left[K_{v\beta_y}\right] = -K_s (A_{55} + A_{66}) \int_{x_i}^{x_f} \left[\Psi'\right]^T [\Psi] dx$$

$$\left[K_{w\beta_x}\right] = K_s (A_{55} + A_{66}) \int_{x_i}^{x_f} \left[\Psi'\right]^T [\Psi] dx \quad \left[K_{w\beta_y}\right] = \left(-\frac{1}{2} K_s B_{16}\right) \int_{x_i}^{x_f} \left[\Psi'\right]^T \left[\Psi'\right] dx$$

$$\left[K_{\beta_x\beta_y}\right] = \frac{1}{2} K_s B_{16} \int_{x_i}^{x_f} \left\{ \left[\Psi'\right]^T [\Psi] - [\Psi]^T \left[\Psi'\right] \right\} dx$$

Damping Matrix of Bearing:

$$\left[C_e^B\right]=\begin{bmatrix}[C_v]_{3\times3} & [0]_{3\times3} & [0]_{3\times3} & [0]_{3\times3}\\ [0]_{3\times3} & [C_w]_{3\times3} & [0]_{3\times3} & [0]_{3\times3}\\ [0]_{3\times3} & [0]_{3\times3} & [0]_{3\times3} & [0]_{3\times3}\\ [0]_{3\times3} & [0]_{3\times3} & [0]_{3\times3} & [0]_{3\times3}\end{bmatrix}_{12\times12}$$

$$[C_v]=\int_{x_i}^{x_f}\sum_{i=1}^{N_B}C_{yy}^{Bi}[\Psi]^T[\Psi]\Delta(x-x_{Bi})dx \quad [C_w]=\int_{x_i}^{x_f}\sum_{i=1}^{N_B}C_{zz}^{Bi}[\Psi]^T[\Psi]\Delta(x-x_{Bi})dx$$

Gyroscopic Matrix:

$$[G_e]=\begin{bmatrix}[0]_{3\times3} & [0]_{3\times3} & [0]_{3\times3} & [0]_{3\times3}\\ [0]_{3\times3} & [0]_{3\times3} & [0]_{3\times3} & [0]_{3\times3}\\ [0]_{3\times3} & [0]_{3\times3} & [0]_{3\times3} & \left[G_{\beta_x\beta_y}\right]_{3\times3}\\ [0]_{3\times3} & [0]_{3\times3} & \left[-G_{\beta_x\beta_y}\right]_{3\times3}^T & [0]_{3\times3}\end{bmatrix}_{12\times12}$$

$$\left[G_{\beta_x\beta_y}\right]=I_P\int_{x_i}^{x_f}[\Psi]^T[\Psi]dx+I_P^D\int_{x_i}^{x_f}\sum_{i=1}^{N_D}[\Psi]^T[\Psi]\Delta(x-x_{Di})dx$$

Elemental circulation matrix $\left[K_{Cir}\right]_{12\times12}=\int_{x_i}^{x_f}M^T\xi M dx$

Where,

$$M=\begin{bmatrix}\psi_1' & \psi_2' & \psi_3' & 0 & 0 & 0 & 0 & 0 & 0 & \psi_1' & \psi_2' & \psi_3'\\ 0 & 0 & 0 & \psi_1' & \psi_2' & \psi_3' & -\psi_1' & -\psi_2' & -\psi_3' & 0 & 0 & 0\\ 0 & 0 & 0 & \psi_1'' & \psi_2'' & \psi_3'' & -\psi_1'' & -\psi_2'' & -\psi_3'' & 0 & 0 & 0\\ \psi_1'' & \psi_2'' & \psi_3'' & 0 & 0 & 0 & 0 & 0 & 0 & \psi_1'' & \psi_2'' & \psi_3''\end{bmatrix}_{4\times12}$$

$$\xi=\begin{bmatrix}0 & GA & 0 & 0\\ -GA & 0 & 0 & 0\\ 0 & 0 & 0 & EI\\ 0 & 0 & -EI & 0\end{bmatrix}_{4\times4}$$

References

[1] Koizumi, M., 1993, "Concept of FGM," Ceramic Trans., **34, pp.** 3–10.

[2] Zinberg, H., Symonds, M.F., 1970, "The Development of an Advanced Composite Tail Rotor Driveshaft," Presented at the 26th Annual Forum of the American helicopter Society, Washington, D.C, June.

[3] Nelson, H.D., Mcvaugh, J.M., 1976, "The dynamics of rotor-bearing systems using finite element method," Journal of Engineering for Industry, **98**, **pp.** 593–600.

[4] Nelson, H.D., 1980, "A finite rotating shaft element using Timoshenko beam element, **102, pp.** 793-803.

[5] Rouch, K.E., Kao, J.S., 1979, "A tapered beam finite element for rotor dynamics analysis," Journal of Sound and Vibration, **66(1), pp.**119-140.

[6] Zorzi, E.S., Nelson, H.D., 1980, "The dynamic of Rotor-bearing systems with axial torque a finite element approach," Journal of Mechanical Design, **102**, **pp.** 158-161.

[7] Bert, C.W., 1992, "The effect of bending–twisting coupling on the critical speed of a driveshafts," Proceedings of the 6th Japan-US Conference on Composite Materials, Orlando, FL. Technomic, Lancaster, PA, **pp.** 29-36.

[8] Kim, C.D., Bert, C.W., 1993, "Critical speed analysis of laminated composite hollow drive shaft," Composite engineering, **3(7-8), pp.** 633-643.

[9] Abramovich, H., Livshits, A., 1993, "Dynamic behavior of cross-ply laminated beams with piezoelectric layers," Composite Structures, **25, pp.** 371-379.

[10] Bert, C.W., Kim, C.D., 1995, "Whirling of composite material driveshaft including bending, twisting coupling and transverse shear deformation," Journal of Vibration and Acoustics, **117, pp.** 17-21.

[11] Bert, C.W., Kim, C.D., 1995, "Dynamic instability of composite-material drive shaft subjected to fluctuating torque and/or rotational speed," Dynamics and Stability of Systems, **2, pp.** 125-147.

[12] Singh, S.P., Gupta, K, 1996, "Composite shaft rotor dynamic analysis using layer wise theory," Journal of Sound and Vibration, **191(5), pp.** 739-756.

[13] Singh, S.P., Gupta, K., 1996, "Dynamic Analysis of composite rotors," International Journal of Rotating Machinery, **2(3), pp.** 179-186.

[14] Forrai, L., 2000, "A finite element model for stability analysis of symmetrical rotor system with internal damping," Journal of Computational and Applied Mechanics, **1 (1), pp.** 37-47.

[15] Chatelet, E., Lornage, D., Jacquet-richardet, G., 2002, "A three dimensional modeling of the dynamic behavior of composite rotors," International Journal of Rotating Machinery, **8(3), pp.** 185-192.

[16] Chang, M.Y., Chen, J.K., Chang, C.Y., 2004, "A simple spinning laminated composite shaft model," International Journal of Solids and Structures, **41, pp.** 637–662.

[17] Kapuria, S., Ahmed, A., Dumir, P.C., 2004, "Static and dynamic thermo electromechanical analysis of angle ply hybrid piezoelectric beams using an efficient coupled zigzag theory," Composites Science and Technology, **64, pp.** 2463–2475.

[18] Gubran, H.B.H., Gupta, K., 2005, "The effect of stacking sequence and coupling mechanisms on the natural frequencies of composite shafts," Journal of Sound and Vibration, **282, pp.** 231-248.

[19] Wang, B.L., Mai, Y.W., 2005, "Transient one dimensional heat conduction problems solved by finite element," International Journal of Mechanical Sciences, **47, pp.** 303-317.

[20] Syed, K.A., Su, C.W., Chan, W.S., 2007, "Analysis of Fiber Reinforced Composite Beams under Temperature Environment," Proceedings of the Seventh International Congress on Thermal Stresses, Taipei, Taiwan.

[21] Sino, R., Baranger, T.N., Chatelet, E., Jacquet, G., 2008, "Dynamic analysis of a rotating composite shaft," Journal of Composites Science and Technology, **68, pp.** 337–345.

[22] Feldman, E., Aboudi, J. 1997, "Buckling analysis of functionally graded plates subjected to uniaxial loading," Composite Structures, **38, pp.** 29–36.

[23] Praveen, G.N.; Reddy, J. N., 1998, "Nonlinear transient thermo elastic analysis of functionally graded ceramic metal plates," International Journal of Solids and Structures, **35(33), pp.** 4457–4476.

[24] Gasik, M.M., 1998, "Micromechanical modeling of functionally graded materials," Computational Materials Science, **13 (1), pp.** 42–55.

[25] Suresh, S., Mortensen, A., 1998, "Fundamentals of functionally graded materials", London, UK: IOM Communications Limited.

[26] Aboudi, J., Pindera, M.J., Arnold, S.M., 1999, "Higher-order theory for functionally graded materials," Composites, Part B: Engineering, **30 (8), pp.**777–832.

[27] Nakamura, T., Wang, T., Sampath, S., 2000, "Determination of properties of graded materials by inverse analysis and instrumented indentation," Acta mater, **48, pp.** 4293–4306.

[28] Wang, B.L., Han, J.C., Du, S.Y., 2000, "Crack problems for Functionally Graded Materials under transient thermal loading," Journal of Thermal Stresses, **23 (2), pp.** 143–168.

[29] Woo, J., Meguid, S. A. 2001, "Nonlinear analysis of functionally graded plates and shallow shells," International Journal of Solids and Structure, **38, pp.** 7409–74021.

[30] Sankar, B. V., 2001, "An elasticity solution for functionally graded beams," Composites Science and Technology, **61, pp.** 689–696.

[31] Sankar, B. V., and Tzeng, J. T. 2002, "Thermal Stresses in Functionally Graded Beams," AIAA Journal, **40(6), pp.** 1228-1232.

[32] Chakraborty, A., Gopalakrishnan, S., Reddy, J. N., 2003, "A New Beam Finite Element for the Analysis of Functionally Graded Materials," International Journal of Mechanical Sciences, **45(3), pp.** 519-539.

[33] Nemta-AIIa, M., 2003, "Reduction of thermal stresses by developing two dimensional functionally graded materials," International journal of solids and structures, **40, pp.** 7339-7356.

[34] Reddy J.N., 1998, "Thermo-mechanical behavior of functionally graded materials," AFOSR Grant F49620-95-1-0342, Washington, D.C, August, **pp.** 1-78.

[35] Na, K. S., Kim, J. H. 2005, "Three-Dimensional Thermo mechanical Buckling of Functionally Graded Materials," AIAA Journal, **43(7), pp.** 1605-1612.

[36] Przybyowicz, Piotr M., 2005, "Stability of activity controlled rotating shaft made of functionally graded materials," Journal of theoretical and applied mechanics, **43(3), pp.** 609-630.

[37] Cooley, William G., 2005. Application of functionally graded materials in aircrafts structures, M.S Thesis, Air Force Institute of Technology, Wright Patterson AFB OH.

[38] Shao, Z.S., 2005, "Mechanical and thermal stresses of a functionally graded circular hollow cylinder with finite length," International Journal of Pressure Vessels and Piping, **82, pp.** 155-163.

[39] WU, Tsung-Lin., Shukla, K.K., Huang, J.H., 2006, "Nonlinear static and dynamic analysis of functionally graded plates," International Journal of applied mechanics and engineering **11(3), pp.** 679-698.

[40] Argeso, H., Eraslan, Ahmet N., 2007, "A Computational Study on Functionally Graded Rotating Solid Shafts," International Journal for Computational Methods in Engineering Science and Mechanics, **8, pp.** 391–399.

[41] Rahimi, G.H., Davoodinik, AR., 2008, "Thermal behavior analysis of the functionally graded Timoshenko's beam," IUST International Journal of Engineering Science, **19(5-1), pp.** 105-113.

[42] Piovan, M.T., Sampaio, R., 2009, "A study on the dynamics of rotating beams with functionally Graded properties," Journal of Sound and Vibration**, 327, pp.** 134-143.

[43] Zhao, X., Lee, Y.Y., Liew, K.M., 2009, "Mechanical and thermal buckling analysis of functionally graded plates," Journal of Composite Structures, **90, pp.** 161-171.

[44] Simsek, M., 2009, "Static analysis of a functionally graded beam under a uniformly distributed load by Ritz method," International Journal of Engineering and Applied Sciences, **1(3), pp.** 1-11.

[45] Giunta, G., Belouettar, S., Carrera, E., 2010, "Analysis of FGM beams by means of classical and advanced theories," Journal of Mechanics of Advanced Materials and Structures, **17, pp.** 622-635.

[46] Afsar, A.M., Go, J., 2010, "Finite element analysis of thermo elastic field in a rotating FGM circular disk, Journal of Applied Mathematical Modelling," **34, pp.** 3309-3320.

[47] Simsek, M., 2010, "Fundamental frequency analysis of functionally graded beams by using different higher order beam theories, Journal of Nuclear Engineering and Design," **240, pp.** 697-705.

[48] Alibeigloo, A., 2010, "Thermo elasticity analysis of functionally graded beam with integrated surface piezoelectric layers," Journal of Composite Structures, **92, pp.** 1535-1543.

[49] Kocaturk,T., Simsek, M., Akbas, S.D., 2011, "Large displacement static analysis of a cantilever Timoshenko beam composed of functionally graded material**,"** Journal of Science and Engineering of Composite Materials**, 18, pp.** 21-34.

[50] Mazzei, Arnaldo J., Scott, Richard A., 2011, "Effect of Functionally Graded Materials on Resonances of Bending Shafts under Time-Dependent Axial Loading," Journal of Vibration and Acoustics, **133, pp.** 061005 (1-10).

[51] Alashti, R. A., Khorsand, M., 2011, "Three-dimensional thermo-elastic analysis of a functionally graded cylindrical shell with piezoelectric layers by differential quadrature method," International Journal of Pressure Vessels and Piping, **88, pp.** 167-180.

[52] Dimentberg, F. M., 1961, "Flexural vibrations of rotating shafts", Butterworths, London.

[53] Gunter, E. J. Jr., Trumpler, P. R., 1969, "The influence of internal friction on the stability of high speed rotors with anisotropic supports," Journal of Engineering for Industry, **pp.** 1105-1113.

[54] Ruhl, R. L., 1970, "Dynamics of distributed parameter rotor systems: transfer matrix and finite element techniques," PhD dissertation, Cornell University.

[55] Ruhl, R.L., Booker, J.F., 1972, "A finite element model for distributed parameter turbo rotor system," Journal of Engineering for Industry, **94(1), pp.** 128-132.

[56] Lund, J. W., 1974, "Stability of damped critical speeds of a flexible rotor in fluid film bearings," Journal of Engineering for Industry, **96, pp.** 509-517.

[57] Dimarogonas, A. D., 1975, "A general method for stability of rotating shafts", Ingenieur Archiv, **44, pp.** 9-20.

[58] Zorzi, E. S., Nelson, H. D.,1977, "Finite element simulation of rotor-bearing systems with internal damping", Journal of Engineering for Power, **pp.**71-76.

[59] Dutt, J. K., Nakra, B. C.,1992, "Stability of rotor systems with viscoelastic supports", Journal of Sound and Vibration, **153(1), pp.** 89-96.

[60] Abduljabbar, Z., EIMadany, M.M., AI-Bahkali, E, 1995, "On the vibration and control of a flexible rotor mounted on fluid film bearing," the fourth Saudi engineering conference Nov., **4, pp.**101-111.

[61] Wettergren, H. L., Olsson, K. O., 1996, "Dynamic instability of a rotating asymmetric shaft with internal viscous damping supported on anisotropic bearings", Journal of Sound and Vibration, **195 (1), pp.** 75-84.

[62] Qin, Q. H., Mao, C. X., 1996, "Coupled torsional-flexural vibration of shaft systems in mechanical engineering-1 finite element model", Journal of Computer & Structures, **58 (4), pp.** 835-843.

[63] Dutt, J. K., Nakra, B. C., 1996, "Stability characteristics of rotating systems with journal bearings on viscoelastic support", Journal of Mechanism and Machine Theory, **31(6), pp.** 771-779.

[64] Ku, D. M., 1998, "Finite element analysis of whirl speeds for rotor-bearing systems with internal damping", Journal of Mechanical Systems and Signal Processing, **12 (5), pp.** 599-610.

[65] Chang, C.Y., Chang, M.Y., Huang, J.H., 2004, "Vibration analysis of rotating composite shafts containing randomly oriented reinforcements," Composite Structures, **63, pp.** 21-32.

[66] Roy, H., Dutt, J.K., Datta, P.K., 2008, "Dynamics of a viscoelastic rotor shaft using augmenting thermodynamic fields-A finite element approach", International Journal of Mechanical Sciences, **50, pp.** 845-853.

[67] Xiang, H.J., Yang, J., 2008, "Free and forced vibration of a laminated FGM Timoshenko beam of variable thickness under heat conduction," Composites: Part B, **39, pp.**292–303.

[68] Li, Q., Iu, V.P., Kou, K.P., 2008, "Three-dimensional vibration analysis of functionally graded material sandwich plates," Journal of Sound and Vibration, **311, pp.** 498 – 515.

[69] Das, A.S., Nighil, M.C., Dutt, J.K.; Irretier, H., 2008, "Vibration control and stability analysis of rotor-shaft system with electromagnetic exciters," Journal of Mechanism and Machine Theory, **43, pp.** 1295–131.

[70] Yang, J., Chen, Y., 2008, "Free vibration and buckling analyses of functionally graded beams with edge cracks". Composite Structures, **83, pp.** 48-60.

[71] Ke, L.L., Yang, J., Kitipornchai, S., Xiang, Y., 2009, "Flexural Vibration and Elastic Buckling of a Cracked Timoshenko Beam Made of Functionally Graded Materials," Journal of Mechanics of Advanced Materials and Structures, **16, pp.** 488–502.

[72] Hosseini, S.A. A., Khadem, S.E., 2009, "Free vibrations analysis of a rotating shaft with nonlinearities in curvature and inertia", Journal of Mechanism and Machine Theory, **44, pp.** 272-288.

[73] Boyaci, A., Seemann, W., Proppe, C., 2009, "Nonlinear stability analysis of rotor-bearing systems," Journal of Proceedings in Applied Mathematics and Mechanics, **9, pp.** 279 -280.

[74] Mahi, A., Adda Bedia, E.A., Tounsi, A., Mechab, I., 2010, "An analytic method for temperature dependent free vibration analysis of functionally graded beams with general boundary conditions," Journal of Composite Structures, **92, pp.** 1877-1887.

[75] Sapountzakis, E. J., Dourakopoulos, J. A., 2010, 'Shear Deformation Effect in Flexural torsional Vibrations of Composite Beams by Boundary Element Method (BEM)," Journal of Vibration and Control, **16, pp.** 1763-1789.

[76] Boukhalfa, A., Hadjoui, A., 2010, "Free vibration analysis of an embarked rotating composite shaft using the hp - version of the FEM," Latin American Journal of Solids and Structures, **7(2), pp.** 105-141.

[77] Kiani, Y., Eslami, M.R., 2010, "Thermal buckling analysis of functionally graded material beams', International Journal of Mechanics and Materials in Design, **6, pp.** 229-238

[78] Shahba, A., Attarnejad, R., Marvi, M. T., Hajilar, S., 2011, "Free vibration and stability analysis of axially functionally graded tapered Timoshenko beams with classical and non-classical boundary conditions," Composites: Part B **42, pp.** 801-808.

[79] Alshorbagy, Amal E., Eltaher, M.A., Mahmoud, F.F., 2011, "Free vibration characteristics of a functionally graded beam by finite element method,' Journal of Applied Mathematical Modelling, **35, pp.** 412-425.

[80] Rafiee, M., Kalhori, H., Mareishi, S., 2011, "Nonlinear resonance analysis of clamped functionally graded beams," 16th International Conference on Composite Structures.

[81] Kumar, J.S., Reddy, B.S., Reddy, C.E., Reddy, K.V.K., 2011, "Higher order theory for free vibration analysis of functionally graded material plates," Journal of Engineering and Applied Sciences, **6 (10), pp.** 105-111.

LIST OF PUBLICATIONS

- **International Journals**

  - Debabrata Gayen and Tarapada Roy, "Hygro-Thermal Effects on Stress Analysis of Tapered Laminated Composite Beam," Int. Journal of Composite Materials, Vol. 3, No. 3, pp. 46-55, 2013, DOI: 10.5923/j.cmaterials.2013030 3.0 2.

  - Debabrata Gayen and Tarapada Roy, "Hygro-Thermal Stress Analysis of Tapered Laminated Composite Beam," Int. Journal of Mechanical Engineering and Research (IJMER), Vol. 3, No. 3, pp. 236-240, 2013.

  - Debabrata Gayen and Tarapada Roy, "Finite Element based Vibration Analysis of Functionally Graded Spinning Shaft System", Int. Journal of Mechanical Sciences. (Submitted)

  - Debabrata Gayen and Tarapada Roy, "Vibration and Stability Analysis of Temperature Dependent Functionally Graded Rotating Shaft System Based on Finite Element Approach", Mechanism and Machine Theory. (To be Submitted)

- **International conferences**

  - Debabrata Gayen, D. Koteswara Rao, Tarapada Roy, "Thermo Mechanical Vibration Analysis of Functionally Graded Rotating Shaft Using Timoshenko Beam Element," 1st Int. Conf. on ICMMME, Goa, 31st March, 2013.

  - D. Koteswara Rao, Tarapada Roy, Debabrata Gayen and Prasad K. Inamdar, "Finite Element Analysis of Functionally Graded Rotor Shaft Using Timoshenko Beam Theory," 2nd Int. Conf. of ICMPE, Hotel Lindsay, Kolkata, 15th February, 2013.